

**RESEARCH ARTICLE**

# Randomized Algorithms for Generalized Singular Value Decomposition with Application to Sensitivity Analysis

Arvind K. Saibaba\*<sup>1</sup> | Joseph Hart<sup>2</sup> | Bart van Bloemen Waanders<sup>2</sup><sup>1</sup>Department of Mathematics, North Carolina State University, North Carolina, USA<sup>2</sup>Optimization and Uncertainty Quantification, Sandia National Laboratories, New Mexico, USA**Correspondence**

\*Arvind K. Saibaba, Department of Mathematics, Box 8205, Raleigh NC, 27695. Email: asaibab@ncsu.edu

**Summary**

The generalized singular value decomposition (GSVD) is a valuable tool that has many applications in computational science. However, computing the GSVD for large-scale problems is challenging. Motivated by applications in hyper-differential sensitivity analysis (HDSA), we propose new randomized algorithms for computing the GSVD which use randomized subspace iteration and weighted QR factorization. Detailed error analysis is given which provides insight into the accuracy of the algorithms and the choice of the algorithmic parameters. We demonstrate the performance of our algorithms on test matrices and a large-scale model problem where HDSA is used to study subsurface flow.

**KEYWORDS:**

Generalized Singular Value Decomposition, Sensitivity Analysis, Randomized Algorithms

## 1 | INTRODUCTION

The singular value decomposition (SVD) is perhaps the most important matrix decomposition from a theoretical and numerical perspective. Applications of the SVD includes image processing (image compression and deblurring), statistics (principal component analysis, canonical correlation analysis), model reduction (proper orthogonal decomposition, discrete empirical interpolation method), and machine learning (principal component analysis).

In this paper, we are concerned with the generalized SVD (GSVD) motivated by an application in hyper-differential sensitivity analysis (HDSA). Two formulations for the GSVD are introduced by van Loan in [21]. The first formulation [21, Theorem 2], which involves a pair of matrices  $\mathbf{A}$ ,  $\mathbf{B}$ , has found application prominently in inverse problems [8] and bioinformatics [1, 14]. The second formulation is the focus of this article and considers a matrix  $\mathbf{A}$  and two matrices,  $\mathbf{S}$  and  $\mathbf{T}$ , which define inner products on the range and column space of  $\mathbf{A}$ , respectively. This formulation, which we refer to as the  $(\mathbf{S}, \mathbf{T})$ -GSVD, arises naturally in a variety of applications including: singular value expansions of compact integral operator (such as Fredholm integral equation of the first kind) [8, Section 2.4], weighted inverse problems [21], uncertainty quantification [18], inverse problems [17], model reduction [4], and hyper-differential sensitivity analysis [9].

In many of the aforementioned applications of the  $(\mathbf{S}, \mathbf{T})$ -GSVD, the matrix  $\mathbf{A}$  arises from discretizing a differential (or integral) equation while  $\mathbf{S}$  and  $\mathbf{T}$  define inner products in the discretized function space(s). These matrices are typically large as a result of the need for fine spatial meshes in two or three dimensions. The size of the resulting matrices and complexity associated with computing matrix-vector products (matvecs) mandates efficient algorithms to enable analysis on otherwise intractable problems. Hence our interest is to develop GSVD algorithms that are efficient and parallelizable. In this paper we analyze randomized algorithms for GSVD which are motivated by and applied to HDSA [9], a recently proposed framework for sensitivity analysis of PDE-constrained optimization solutions, as summarized in Section 2.1.

One approach to computing the  $(\mathbf{S}, \mathbf{T})$ -GSVD is to use the Cholesky (or any other appropriate factorization) of  $\mathbf{S}$  and  $\mathbf{T}$  to transform it into a standard SVD problem. However, computing the Cholesky factorization can be a significant computational bottleneck in large-scale application. A central goal in this paper is to avoid such factorizations of  $\mathbf{S}$  and  $\mathbf{T}$ . Instead, our algorithms only rely on matvecs with  $\mathbf{S}, \mathbf{T}$  or their inverses. This makes our approach matrix-free and hence advantageous for large scale applications.

### Previous work

We briefly review the literature on algorithms for large-scale computation of the GSVD. In previous work [18], a randomized algorithm was developed for generalized Hermitian eigenvalue problems (GHEP) with application to computing the Karhunen-Loève decomposition. The GSVD can be formulated as a GHEP in several different ways (a discussion on this can be found in Section 3.4) and this was used in [9] in the context of sensitivity analysis. In [18], a randomized algorithm for the GSVD was presented but no analysis for this algorithm was shown. In recent work, [24, 22] a randomized algorithm GSVD algorithm for the  $\mathbf{B}$ -GSVD was developed. Here too, there has been no analysis of the randomized algorithms.

### Contributions

This paper makes several contributions for computing large-scale GSVD using randomized algorithms. We give a summary of the main contributions of this paper, while emphasizing the novelty of our approach.

First, in Section 3, we develop new matrix-free randomized algorithms for efficiently computing the truncated GSVD. The algorithms combine weighted QR factorizations with randomized subspace iteration and improve upon the algorithms developed in [18]. A detailed analysis of the computational cost is provided and compared to our algorithms with related formulations based on the GHEP.

Second, in Section 4, we provide detailed probabilistic analysis of the error in the low-rank decompositions. The analysis is new and sheds light on the choice of the algorithmic parameters so that the trade-off between computational cost and accuracy is clear. Motivated by the error analysis, we propose a new algorithm that uses a preconditioner to lower the error in the low-rank approximation.

Third, in Section 5, we show how to efficiently speed up the computations in the HDSA framework using the proposed randomized algorithms. We demonstrate the performance of our algorithms on a large scale model problem in which we seek to control injection wells to meet desired production well fluid pressure profiles, subject to uncertainty in the heterogeneous subsurface media.

## 2 | BACKGROUND AND NOTATION

We begin by overviewing HDSA in Section 2.1 which motivates the large-scale GSVD problem that we tackle in this paper. We review the notation and recall fundamental facts about the SVD and GSVD in 2.2 and the weighted QR decomposition in Section 2.3.

### 2.1 | Hyper-differential sensitivity analysis

HDSA determines the sensitivity of the solution of an optimization problem with respect to fixed parameters. Of particular interest are optimization problems constrained by partial differential equations (PDEs) in the form

$$\begin{aligned} \min_{u, z} J(u, z) \\ \text{s.t. } c(u, z, \theta) = 0 \end{aligned} \quad (1)$$

where  $c(u, z, \theta)$  represent a PDE with state  $u$  and parameters  $\theta$ . In this case, the optimization variable  $z$  may correspond to a system design or control, or an unknown parameter to be determined in an inverse problem. The parameters  $\theta$  may correspond to physical parameters which are uncertain or variable, but out of necessity are fixed to a nominal value in the formulation of (1).

HDSA considers the sensitivity of the solution of (1) to changes in  $\theta$ . To define such sensitivity, let  $z_0$  denote a locally optimal solution of (1) for a specified nominal estimate  $\theta = \theta_0$ . Under mild assumptions, see [9], there exists a function  $z^*(\theta)$  which maps parameters  $\theta$  in a neighborhood of  $\theta_0$  to local minima  $z^*(\theta)$  in a neighborhood of  $z_0$ . The Fréchet derivative of  $z^*$  with

respect to  $\theta$ , which we denote by  $Dz^*$ , is given by

$$Dz^* = \Pi \mathcal{K}^{-1} \mathcal{B}, \quad (2)$$

where  $\Pi$  is a projection operator,  $\mathcal{K}$  is the Karush Kuhn Tucker operator for (1), and  $\mathcal{B}$  is the negative Fréchet derivative of the gradient of the Lagrangian of (1) with respect to  $\theta$ . Computing the action of  $Dz^*$  requires a large linear system solve, applying  $\mathcal{K}^{-1}$ , and each application of the operator  $\mathcal{K}$  requires multiple PDE solves. Hence applying  $Dz^*$  is computationally intensive and we seek to mitigate the number of operator applies.

In general,  $\theta$  and  $z$  are elements of infinite dimensional function spaces  $\Theta$  and  $Z$ , respectively, which we assume to be Hilbert spaces. Upon discretization of the parameters with a finite dimensional basis  $\{\theta_1, \theta_2, \dots, \theta_n\}$ , we define the hyper-differential sensitivity indices

$$S_i = \frac{\|Dz^* \theta_i\|}{\|\theta_i\|} \quad i = 1, 2, \dots, n, \quad (3)$$

where the norms are computed in  $\Theta$  and  $Z$ . As the dimension of the discretized parameter space  $n$  may be large, computing each  $S_i$  through operator applies  $Dz^* \theta_i$ ,  $i = 1, 2, \dots, n$  is prohibitive. An efficient alternative is to compute the GSVD of  $Dz^*$  where the inner products are computed in  $\Theta$  and  $Z$ . If  $Dz^*$  possess low rank structure, which is common in many applications, the indices (3) may be efficiently estimated using the leading singular values and vectors of  $Dz^*$ .

In the notation of Section 1 and the remainder of the paper,  $\mathbf{A} \in \mathbb{R}^{m \times n}$  corresponds to the discretization of  $Dz^*$ . In the scope of HDSA,  $m$  and  $n$  correspond to the dimension of the discretization of  $Z$  and  $\Theta$ , respectively, both of which are typically large (corresponding to discretizations of PDEs). The matrices  $\mathbf{S}$  (not to be confused with the sensitivity index  $S_i$ ) and  $\mathbf{T}$  encode the function space inner products and their dimensions are likewise dependent on discretizations of PDEs. For HDSA,  $\mathbf{A}$  will be large, dense, and only accessible through matvecs which require many PDE solves per matvec, hence our motivation for efficient and parallel algorithms. In most cases,  $\mathbf{S}$  and  $\mathbf{T}$  will be large and sparse. Matvecs with  $\mathbf{S}$  and  $\mathbf{T}$  are less computationally intensive than with  $\mathbf{A}$  (they do not require PDE solves), but factorizations of  $\mathbf{S}$  and  $\mathbf{T}$  are undesirable because of their size and the loss of sparsity that typically results.

## 2.2 | SVD and GSVD

Given a positive definite matrix  $\mathbf{M} \in \mathbb{R}^{n \times n}$  and  $\mathbf{x} \in \mathbb{R}^n$ , we define the weighted inner product  $\langle \mathbf{x}, \mathbf{y} \rangle_{\mathbf{M}} = \mathbf{x}^T \mathbf{M} \mathbf{y}$  and the associated vector norm

$$\|\mathbf{x}\|_{\mathbf{M}} = \sqrt{\mathbf{x}^T \mathbf{M} \mathbf{x}} = \|\mathbf{M}^{1/2} \mathbf{x}\|_2 = \|\mathbf{L}_{\mathbf{M}}^T \mathbf{x}\|_2,$$

where  $\mathbf{M}^{1/2}$  is the matrix square root and  $\mathbf{L}_{\mathbf{M}}$  is the (lower) Cholesky factor of  $\mathbf{M}$ , i.e.,  $\mathbf{M} = \mathbf{L}_{\mathbf{M}} \mathbf{L}_{\mathbf{M}}^T$ . Let  $\mathbf{A} \in \mathbb{R}^{m \times n}$  and let  $\mathbf{S} \in \mathbb{R}^{m \times m}$  and  $\mathbf{T} \in \mathbb{R}^{n \times n}$  be symmetric positive definite matrices. The induced matrix norm is

$$\|\mathbf{A}\|_{\mathbf{T} \rightarrow \mathbf{S}} = \max_{\mathbf{x} \neq 0} \frac{\|\mathbf{A} \mathbf{x}\|_{\mathbf{S}}}{\|\mathbf{x}\|_{\mathbf{T}}} = \|\mathbf{L}_{\mathbf{S}}^T \mathbf{A} \mathbf{L}_{\mathbf{T}}^{-T}\|_2,$$

where  $\|\cdot\|_2$  is the spectral norm and  $\mathbf{L}_{\mathbf{S}}$  and  $\mathbf{L}_{\mathbf{T}}$  are the (lower) Cholesky factorizations of  $\mathbf{S}$  and  $\mathbf{T}$  respectively. In the proofs, it will be convenient to use the alternative relation

$$\|\mathbf{A}\|_{\mathbf{T} \rightarrow \mathbf{S}} = \|\mathbf{S}^{1/2} \mathbf{A} \mathbf{T}^{-1/2}\|_2.$$

where  $\mathbf{S}^{1/2}$  and  $\mathbf{T}^{1/2}$  are the matrix square root of  $\mathbf{S}$  and  $\mathbf{T}$  respectively; however, the Cholesky formulation is preferable from a computational point of view. We denote by  $\kappa_2(\mathbf{T}) = \|\mathbf{T}\|_2 \|\mathbf{T}^{-1}\|_2$ , the condition number of inversion in the spectral norm.

Following the  $(\mathbf{S}, \mathbf{T})$ -GSVD formulation from [21], there exist matrices  $\mathbf{U} \in \mathbb{R}^{m \times m}$  that is  $\mathbf{S}$ -orthogonal, i.e.,  $\mathbf{U}^T \mathbf{S} \mathbf{U} = \mathbf{I}$  and  $\mathbf{V}$  that is  $\mathbf{T}$ -orthogonal such that

$$\mathbf{U}^{-1} \mathbf{A} \mathbf{V} = \mathbf{\Sigma},$$

where  $\mathbf{\Sigma} \in \mathbb{R}^{m \times n}$  is a diagonal matrix containing the generalized singular values (in decreasing order)

$$\sigma_1 \geq \sigma_2 \geq \dots \geq \sigma_{\min\{m,n\}} \geq 0.$$

Alternatively, since  $\mathbf{V}^{-1} = \mathbf{V}^T \mathbf{T}$ , we can write

$$\mathbf{A} = \mathbf{U} \mathbf{\Sigma} \mathbf{V}^T \mathbf{T}. \quad (4)$$

For a target rank  $k \leq \text{rank}(\mathbf{A})$ , we can partition the GSVD (4) as

$$\mathbf{A} = [\mathbf{U}_k \ \mathbf{U}_\perp] \begin{bmatrix} \boldsymbol{\Sigma}_k & \\ & \boldsymbol{\Sigma}_\perp \end{bmatrix} \begin{bmatrix} \mathbf{V}_k^\top \mathbf{T} \\ \mathbf{V}_\perp^\top \mathbf{T} \end{bmatrix},$$

where  $\mathbf{U}_k \in \mathbb{R}^{m \times k}$ ,  $\mathbf{V}_k \in \mathbb{R}^{n \times k}$  and  $\boldsymbol{\Sigma}_k \in \mathbb{R}^{k \times k}$ . This form will be useful in the error analysis.

By contrast, consider the standard SVD of  $\mathbf{A} = \mathbf{W} \mathbf{S}_A \mathbf{Z}^\top$ , where  $\mathbf{W} \in \mathbb{R}^{m \times m}$  and  $\mathbf{Z} \in \mathbb{R}^{n \times n}$  are orthogonal, whose columns respectively contain the left and right singular values, and  $\mathbf{S}_A \in \mathbb{R}^{m \times n}$  is a diagonal matrix containing the singular values (in decreasing order)

$$s_1 \geq s_2 \geq \dots \geq s_{\min\{m,n\}} \geq 0.$$

Letting  $s_j(\mathbf{A})$  and  $\sigma_j(\mathbf{A})$  denote the  $j^{\text{th}}$  singular value and generalized singular value of  $\mathbf{A}$ , respectively. We observe that the generalized singular values of  $\mathbf{A}$  equal the singular values of  $\mathbf{L}_S^\top \mathbf{A} \mathbf{L}_T^{-\top}$ , i.e.,

$$\sigma_j(\mathbf{A}) = s_j(\mathbf{L}_S^\top \mathbf{A} \mathbf{L}_T^{-\top}), \quad j = 1, \dots, \min\{m, n\}.$$

The generalized left singular vectors of  $\mathbf{A}$  can be obtained as  $\mathbf{U} = \mathbf{L}_S^{-\top} \mathbf{W}$  and the generalized right singular vectors can be obtained as  $\mathbf{V} = \mathbf{L}_T^{-\top} \mathbf{Z}$ . It is easy to verify that  $\mathbf{U}$  and  $\mathbf{V}$  are  $\mathbf{S}$ - and  $\mathbf{T}$ -orthogonal, respectively. The details are in [21, Theorem 3]. Furthermore, the multiplicative singular value inequalities [10, Equation (7.3.14)] imply

$$\frac{s_j(\mathbf{A})}{\sqrt{\|\mathbf{S}^{-1}\|_2 \|\mathbf{T}\|_2}} \leq \sigma_j(\mathbf{A}) \leq \sqrt{\|\mathbf{S}\|_2 \|\mathbf{T}^{-1}\|_2} s_j(\mathbf{A}) \quad j = 1, \dots, \min\{m, n\}.$$

This bound shows that the generalized singular values and the singular values may be substantially different, if  $\mathbf{S} \neq \mathbf{I}_m$  and/or  $\mathbf{T} \neq \mathbf{I}_n$ .

### 2.3 | QR in a weighted inner product

An important algorithmic component for the randomized algorithm is an efficient way of computing the thin QR factorization in the weighted inner product. We review the ‘PreCholQR’ algorithm described in [13, Algorithm 2]; we call this algorithm Weighted CholQR. Given a positive definite matrix  $\mathbf{W} \in \mathbb{R}^{m \times m}$ , this algorithm produces a QR factorization of  $\mathbf{Z} \in \mathbb{R}^{m \times n}$  with  $m \geq n$  such that

$$\mathbf{Z} = \mathbf{Q} \mathbf{R} \quad \mathbf{Q}^\top \mathbf{W} \mathbf{Q} = \mathbf{I}_n,$$

and  $\mathbf{R} \in \mathbb{R}^{n \times n}$  is an upper triangular matrix. See Algorithm 1 for the implementation details.

**Input:** Matrix  $\mathbf{Z} \in \mathbb{R}^{m \times n}$  with  $m \geq n$  and positive definite matrix  $\mathbf{W} \in \mathbb{R}^{m \times m}$ .

**Output:** Matrices  $\mathbf{Q} \in \mathbb{R}^{m \times n}$  and  $\mathbf{R} \in \mathbb{R}^{n \times n}$  satisfying  $\mathbf{Z} = \mathbf{Q} \mathbf{R}$  with  $\mathbf{Q}^\top \mathbf{W} \mathbf{Q} = \mathbf{I}$ .

/\* Call this function as:  $[\mathbf{Q}, \mathbf{R}] = \text{CholQR}(\mathbf{Z}, \mathbf{W})$ . \*/

- 1 Compute thin QR factorization  $\mathbf{Q}_Z \mathbf{R}_Z = \mathbf{Z}$
- 2 Compute  $\mathbf{Q}_W = \mathbf{W} \mathbf{Q}_Z$  Compute the Cholesky factorization of  $\mathbf{Q}_Z^\top \mathbf{Q}_W = \mathbf{R}_W^\top \mathbf{R}_W$
- 3 Form  $\mathbf{R} = \mathbf{R}_W \mathbf{R}_Z$  and  $\mathbf{Q} = \mathbf{Q}_Z \mathbf{R}_W^{-1}$

**Algorithm 1:** Weighted CholQR.

In addition to computing  $\mathbf{Q}$ , we may have to also compute  $\mathbf{W} \mathbf{Q}$ ; from Algorithm 1, we see that it equals  $\mathbf{Q}_W \mathbf{R}_W^{-1}$ . This way, we can compute  $\mathbf{W} \mathbf{Q}$  without expending additional matvecs with  $\mathbf{W}$ . The computational cost of Algorithm 1 can be summarized as:  $k$  matvecs involving  $\mathbf{W}$  and an additional  $\mathcal{O}(nk^2)$  floating point operations (flops). In practice, we use a modification of Algorithm 1. This modified algorithm first computes a thin-QR factorization of  $\mathbf{Z}$  before applying Algorithm 1. See [13, Section 3] for a discussion on this algorithm.

We will also need to use projection matrices in weighted inner products. Let  $\mathbf{A}^\dagger$  denote the Moore-Penrose inverse of  $\mathbf{A}$ . The orthogonal projector onto the range of  $\mathbf{A}$  is denoted as  $\boldsymbol{\Pi}_A = \mathbf{A} \mathbf{A}^\dagger$ . If  $\mathbf{Q} \in \mathbb{R}^{m \times k}$  has  $\mathbf{S}$ -orthonormal columns, i.e.,  $\mathbf{Q}^\top \mathbf{S} \mathbf{Q} = \mathbf{I}_k$ , then  $\boldsymbol{\Pi}_Q = \mathbf{Q} \mathbf{Q}^\dagger = \mathbf{Q} \mathbf{Q}^\top \mathbf{S}$ .

### 3 | ALGORITHMS

In Section 3.1 we propose the basic version of the randomized algorithm for GSVD. Next, in Section 3.2, we propose a randomized algorithm for GSVD based on subspace iteration, with special attention to handling the weighted inner products. A discussion on the computational cost of these algorithms is presented in Section 3.3 and we end this section with alternative ways of computing the GSVD by formulating it as a generalized hermitian eigenvalue problem (GHEP) Section 3.4.

#### 3.1 | Outline of the Basic algorithm

We first give an informal description of the basic version of the algorithm that helps highlight the overall structure. We call this algorithm basic, since it will be a special case of the more general algorithm in Section 3.2. The basic algorithm is comprised of two stages:

**Stage 1:** determine a subspace to approximate the range of  $\mathbf{A}$  by randomized sampling,

**Stage 2:** compute a low rank approximation of  $\mathbf{A}$  by projecting on to the subspace determined in Stage 1 and convert into GSVD format.

An optional postprocessing step truncates the decomposition to the desired target rank  $k$ .

To execute Stage 1, we draw a random matrix  $\mathbf{\Omega} \in \mathbb{R}^{n \times (k+p)}$ , where  $k$  is the target rank,  $p \geq 0$  is an oversampling parameter that can be used to control the accuracy of the low-rank approximation, and  $\ell \equiv k + p \leq \min\{m, n\}$ . The specific choice of the distribution of  $\mathbf{\Omega}$  will not be discussed at this point; see the end of Section 3.3. The next step is to compute  $\mathbf{Y} = \mathbf{A}\mathbf{\Omega}$  and a basis for its range. Specifically, we use the weighted CholQR described in Algorithm 1 with  $\mathbf{W} = \mathbf{S}$ . We then have  $\mathbf{Y} = \mathbf{Q}\mathbf{R}$  and  $\mathbf{Q}^\top \mathbf{S}\mathbf{Q} = \mathbf{I}_\ell$ .

In Stage 2, we can obtain a low-rank approximation of the form

$$\mathbf{A} \approx \mathbf{Q}\mathbf{Q}^\top \mathbf{S}\mathbf{A} = \mathbf{\Pi}_\mathbf{Q}\mathbf{A},$$

where  $\mathbf{\Pi}_\mathbf{Q} \equiv \mathbf{Q}\mathbf{Q}^\top \mathbf{S}$  is an  $\mathbf{S}$ -orthogonal projector. That is, to obtain a low-rank approximation, we project  $\mathbf{A}$  onto the range of  $\mathbf{Q}$ . A few additional steps are then used to convert this low-rank approximation into the GSVD format

$$\mathbf{A} \approx \mathbf{\Pi}_\mathbf{Q}\mathbf{A} = \widehat{\mathbf{U}}\widehat{\mathbf{\Sigma}}\widehat{\mathbf{V}}^\top \mathbf{T}.$$

We now present a method for improved accuracy by using randomized subspace iteration in Stage 1. We can view the basic algorithm, outlined above, as a special case of Algorithm 3 with  $q = 0$  steps of the subspace iteration.

#### 3.2 | Improved accuracy via subspace iteration

**Input:** Matrices  $\mathbf{A} \in \mathbb{R}^{m \times n}$ ,  $\mathbf{S} \in \mathbb{R}^{m \times m}$  and  $\mathbf{T} \in \mathbb{R}^{n \times n}$ . Random Matrix  $\mathbf{\Omega} \in \mathbb{R}^{n \times \ell}$  such that  $\ell \leq \min\{m, n\}$

**Output:** Matrices  $\mathbf{Q} \in \mathbb{R}^{n \times \ell}$  such that  $\mathbf{Q}^\top \mathbf{S}\mathbf{Q} = \mathbf{I}_\ell$ .

```

/* Call as: [Q] = RandSubspace(A, S, T, Omega, q). */
1 Compute Y = A*Omega.
2 Compute [Q, R] = CholQR(Y, S).
3 for j = 1, ..., q do
4     Update sketch Y = A^T * S * Q.
5     Compute [Q, R] = CholQR(Y, T^-1).
6     Update sketch Y = A * T^-1 * Q.
7     Compute [Q, R] = CholQR(Y, S).
8 end

```

**Algorithm 2:** Randomized subspace iteration with weighted inner products.

Stage 1 of the basic algorithm may be executed with Lines 1-2 in Algorithm 3. Subspace iteration augments them with Lines 3-8 (in Algorithm 3) to attain a better projector via the “sketch”

$$Y = (AT^{-1}A^T S)^q A \Omega,$$

where  $q \geq 0$  is the number of subspace iterations. The rationale behind this sketch is clear if we plug in the generalized SVD  $A = U \Sigma V^T T$  to obtain

$$Y = U(\Sigma \Sigma^T)^q \Sigma V^T T \Omega. \quad (5)$$

Analytical error bounds and numerical evidence shows that employing subspace iterations improves upon the accuracy of the basic algorithm in Section 3.1. A naive implementation of the subspace iteration as in Eq. (5), can have poor behavior in the presence of round-off error. This can be addressed by alternating QR factorizations with products involving  $A$  and  $A^T$ . We present a version of the subspace iterations in Algorithm 2 that accounts for weighted inner products. The randomized subspace iteration produces a matrix  $Q \in \mathbb{R}^{m \times \ell}$  with  $S$ -orthonormal columns, which approximates  $\text{range}(A)$  and  $A \approx Q Q^T S A$ . This low-rank approximation can be converted into an approximate  $(S, T)$ -GSVD format by employing Stage 2 of Algorithm 3.

**Input:** Matrix  $A \in \mathbb{R}^{m \times n}$ . Target rank  $k \leq \text{rank}(A)$ , oversampling parameter  $p \geq 0$ , such that  $\ell = k + p \leq \min\{m, n\}$ .

**Output:** Matrices  $\hat{U}, \hat{\Sigma}, \hat{V}$  such that  $A \approx \hat{U} \hat{\Sigma} \hat{V}^T T$ .

```
// Stage 1: Range finder.
1 Draw random matrix  $\Omega \in \mathbb{R}^{n \times \ell}$ .
2 Apply subspace iteration  $[Q] = \text{RandSubspace}(A, S, T, \Omega, q)$ .
// Stage 2: Computing a low-rank factorization.
3 Compute  $B = A^T S Q$ .
4 Compute the QR factorization  $[Q_B, R_B] = \text{CholQR}(T^{-1} B^T, T)$ .
5 Compute the SVD of  $R_B^T = U_B \hat{\Sigma} V_B^T$ .
6 Compute  $\hat{U} = Q U_B$  and  $\hat{V} = Q_B V_B$ .
7 Truncation step (optional):  $\hat{U} = \hat{U}(:, 1:k)$ ,  $\hat{\Sigma} = \hat{\Sigma}(1:k, 1:k)$  and  $\hat{V} = \hat{V}(:, 1:k)$ .
```

**Algorithm 3:** Randomized generalized SVD.

We will see from the analysis in Section 4, that the basic version of the randomized algorithm is accurate when  $T$  is well conditioned and the generalized singular values  $\sigma_j$ , with index  $j > k$  are sufficiently small. The number of subspace iterations  $q$  involve a trade-off between computational costs and accuracy, and depend on the decay of the generalized singular values the condition number of  $T$ .

### 3.3 | Computational cost and alternative formulations

We now summarize the computational cost of the randomized GSVD using the subspace iteration. Let  $q$  denote the number of subspace iterations, and  $\ell$  be the number of columns of  $\Omega$ . The cost in Stage 1 is dominated by the steps in Algorithm 2. From Eq. (5), it is clear that we perform  $(q + 1)\ell$  products with  $A$ , and  $q\ell$  matvecs with  $A^T$ . Additionally, we have to perform  $q\ell$  matvecs with  $S$  and  $q\ell$  matvecs with  $T^{-1}$  (or solves with  $T$ ). The weighted QR involving  $S$  requires  $\mathcal{O}(k^2 m)$  flops and those involving  $T$  require  $\mathcal{O}(k^2 n)$  flops. We now discuss the cost in Stage 2. Step 4 requires  $\ell$  matvecs with  $A^T$  and  $S$  respectively; Step 5 requires  $\ell$  matvecs with  $T^{-1}$  and  $T$  and an additional cost of  $\mathcal{O}(nk^2)$  flops. Steps 6 and 7 require  $\mathcal{O}(k^2(m + n))$  flops. A summary of this discussion is available in Table 1.

**Should one use  $A$  or  $A^T$ ?**

One can, in principle, apply Algorithm 3 (appropriately modified using subspace iteration) to  $A^T$  yielding the approximate  $(T^{-1}, S^{-1})$  GSVD

$$A^T \approx \hat{X} \hat{\Sigma} \hat{Y}^T S^{-1},$$

Stage	$\mathbf{Ax}$	$\mathbf{A}^\top \mathbf{x}$	$\mathbf{Sx}$	$\mathbf{Tx}$	$\mathbf{T}^{-1} \mathbf{x}$	Other flops
Range find.	$(q+1)\ell$	$q\ell$	$q\ell$	–	$q\ell$	$\mathcal{O}(qk^2(m+n))$
Low-rank fact.	–	$\ell$	$\ell$	$\ell$	$\ell$	$\mathcal{O}(k^3 + k^2(m+n))$

**TABLE 1** The computational cost of the randomized GSVD algorithm with subspace iteration. Here,  $m$  and  $n$  refers to the size of  $\mathbf{A}$ ,  $k$  is the target rank,  $\ell = k + p$ , where  $p \geq 0$  is the oversampling parameter, and  $q \geq 0$  is the number of subspace iterations.

where  $\hat{\mathbf{X}}$  has  $\mathbf{T}^{-1}$ -orthonormal columns and  $\hat{\mathbf{Y}}$  has  $\mathbf{S}^{-1}$ -orthonormal columns. The singular values contained in  $\hat{\mathbf{\Sigma}}$  approximate the singular values in  $\mathbf{T}^{-1/2} \mathbf{A}^\top \mathbf{S}^{1/2}$ , as desired. To obtain the  $(\mathbf{S}, \mathbf{T})$ -GSVD of  $\mathbf{A}$ , we first observe

$$\mathbf{A} \approx \mathbf{S}^{-1} \hat{\mathbf{Y}} \hat{\mathbf{\Sigma}} \hat{\mathbf{X}}^\top.$$

Then, we make the transformation  $\hat{\mathbf{U}} = \mathbf{S}^{-1} \hat{\mathbf{Y}}$  (which has  $\mathbf{S}$ -orthonormal columns) and  $\hat{\mathbf{V}} = \mathbf{T}^{-1} \hat{\mathbf{X}}$  (which has  $\mathbf{T}$ -orthonormal columns), giving the approximate  $(\mathbf{S}, \mathbf{T})$  GSVD  $\mathbf{A} \approx \hat{\mathbf{U}} \hat{\mathbf{\Sigma}} \hat{\mathbf{V}}^\top \mathbf{T}$ . However, it is immediately clear that we have to perform solves with  $\mathbf{S}$  (alternatively, matvecs with  $\mathbf{S}^{-1}$ ). If solves with  $\mathbf{S}$  is cheaper than solves with  $\mathbf{T}$  (which is required by Algorithm 3), then it maybe preferable to use this alternative formulation. Another reason to prefer this alternative formulation is if  $\mathbf{S}$  has a lower condition number than  $\mathbf{T}$ ; that is,  $\kappa_2(\mathbf{S}) < \kappa_2(\mathbf{T})$ . The reason is that the error analysis in Theorem 3, shows an explicit dependence on the condition number  $\kappa_2(\mathbf{T})$ ; the alternative formulation would involve  $\kappa_2(\mathbf{S})$  and therefore may have higher accuracy.

### Choice of $\mathbf{\Omega}$

In Sections 3.1 and 3.2, we left the choice of the random matrix  $\mathbf{\Omega}$  unspecified. We briefly comment on the possible choices. A popular choice, we adopt in this paper, is to take  $\mathbf{\Omega}$  to be a standard Gaussian random matrix. That is, with entries are independent and identically distributed (i.i.d) Gaussian random variables with mean 0 and variance 1. This choice of  $\mathbf{\Omega}$  ensures that the amount of oversampling needed in practice can be quite modest. For example, following the arguments in [6, Equation (5.9)], we can take  $p = 20$ . Other choices are possible, such as subsampled randomized Hadamard/Fourier transform (SRHT/SRFT), Rademacher random matrices, sparse Rademacher random matrices, etc. A discussion of these choice has been provided in [7, Section 4.6] and [20, Section 3.9]. In Section 4.3, we propose a different approach for constructing the random matrix  $\mathbf{\Omega}$ , that makes use of a preconditioner for  $\mathbf{T}$ .

## 3.4 | Computing GSVD using GHEP

There are three alternatives approaches to compute the GSVD by casting it as a GHEP. In the first approach, we consider the GHEP  $\mathbf{A}^\top \mathbf{S} \mathbf{A} \mathbf{x} = \lambda \mathbf{T} \mathbf{x}$ . The second approach considers a similar GHEP,  $\mathbf{A} \mathbf{T}^{-1} \mathbf{A} \mathbf{x} = \lambda \mathbf{S}^{-1} \mathbf{x}$ . In both approaches, the left and right generalized singular vectors can be extracted from the generalized eigenvectors but require additional matvecs with  $\mathbf{A}$  or  $\mathbf{A}^\top$ . The third approach considers the Jordan-Wielandt-type augmented matrix

$$\begin{bmatrix} \mathbf{A} & \mathbf{A} \\ \mathbf{A}^\top & \mathbf{A} \end{bmatrix} \begin{bmatrix} \mathbf{x} \\ \mathbf{y} \end{bmatrix} = \lambda \begin{bmatrix} \mathbf{S}^{-1} & \\ & \mathbf{T} \end{bmatrix} \begin{bmatrix} \mathbf{x} \\ \mathbf{y} \end{bmatrix}. \quad (6)$$

In our previous work [18], we proposed randomized algorithms for GHEP. In principle, we can compute an  $(\mathbf{S}, \mathbf{T})$ -GSVD using any of the three formulations described above. However, there are several reasons to use the proposed algorithms in this paper:

- Algorithm 3 is mathematically simpler because it approximates the GSVD directly rather than reformulating it as a GHEP and post-processing the generalized eigenvalues/vectors.
- The first two formulations, which involve working with  $\mathbf{A}^\top \mathbf{S} \mathbf{A}$  and  $\mathbf{A} \mathbf{T}^{-1} \mathbf{A}$ , can lead to a loss in accuracy, especially when estimating the smallest singular values; see discussion in [2, Section 2.1.4] and [12, Section 3.2] for more details.
- The cost of the randomized GHEP using the first two formulations is, roughly speaking, twice as expensive as Algorithm 3 with  $q = 0$  since it would require  $2\ell$  matvecs with  $\mathbf{A}$  and  $\mathbf{A}^\top$ ; however, the cost is (nearly) comparable to Algorithm 3 with  $q = 1$ . The results presented in Section 5 show that the proposed algorithm is more accurate than the GHEP approach for a comparable computational budget.

- The generalized eigenvalues in the third approach come in pairs of positive and negative eigenvalues of equal magnitude. To compute the  $k$  largest positive eigenvalues (needed to estimate the GSVD) with a randomized solver requires computing  $2k$  eigenvalues. Additionally, while the generalized eigenvectors are orthogonal up to numerical precision, the components ( $\mathbf{x}$  and  $\mathbf{y}$  in (6)) which determine the left and right generalized singular vectors may not be orthogonal in practice, particularly those corresponding to smaller singular values.

## 4 | ANALYSIS

We present error bounds that give insight into the accuracy of the randomized algorithms for computing the GSVD developed in the previous section. The strategy for the analysis is split into two different stages: deterministic or “structural” in which, we make minimal assumptions regarding the distribution of the random matrix  $\mathbf{\Omega}$  (Section 4.1), and probabilistic, in which we specialize the results to specific distributions of  $\mathbf{\Omega}$  (Section 4.2). In Section 4.4, we also provide analysis of the randomized algorithm for the GHEP.

### 4.1 | Deterministic analysis

We assume that the target rank  $1 \leq k \leq \text{rank}(\mathbf{A})$  and define the singular value ratio

$$\gamma_k \equiv \frac{\sigma_{k+1}}{\sigma_k}.$$

The gap between the singular values  $\sigma_k$  and  $\sigma_{k+1}$  is the inverse of the singular value ratio  $\gamma_k$ . In applications of interest, there may be a large singular value gap which may be exploited to accelerate the convergence of the subspace iteration. Let us turn our attention to the matrix  $\mathbf{\Omega} \in \mathbb{R}^{n \times \ell}$  and define

$$\hat{\mathbf{\Omega}}_1 \equiv \mathbf{V}_k^\top \mathbf{T} \mathbf{\Omega} \quad \hat{\mathbf{\Omega}}_2 \equiv \mathbf{V}_\perp^\top \mathbf{T} \mathbf{\Omega} \quad (7)$$

The following is the only assumption we make on the random matrix  $\mathbf{\Omega}$

$$\text{rank}(\hat{\mathbf{\Omega}}_1) = k. \quad (8)$$

This assumption ensures that  $\hat{\mathbf{\Omega}}_1 \in \mathbb{R}^{k \times \ell}$  has full row-rank and therefore has a right multiplicative inverse, i.e.,  $\hat{\mathbf{\Omega}}_1 \hat{\mathbf{\Omega}}_1^\dagger = \mathbf{I}_k$ .

We present two different types of bounds for the analysis of the randomized subspace iteration. The first bound is gap-dependent and shows explicit dependence on  $\gamma_k$ , the ratio of the singular values  $\sigma_k$  and  $\sigma_{k+1}$ , whereas the second bound called gap-independent does not depend on  $\gamma_k$ . We also recall some basic properties that will be needed in our analysis. Let  $\mathbf{C}, \mathbf{D} \in \mathbb{R}^{n \times n}$  be symmetric. The notation  $\mathbf{C} \leq \mathbf{D}$  means  $\mathbf{D} - \mathbf{C}$  is positive semidefinite. Let  $\mathbf{M}, \mathbf{N}$  be two matrices with the same number of rows and let  $\text{range}(\mathbf{N}) \subset \text{range}(\mathbf{M})$ ; then by [7, Proposition 8.4]  $\mathbf{\Pi}_N \leq \mathbf{\Pi}_M$ . Furthermore,

$$\|\mathbf{\Pi}_N \mathbf{A}\|_2 \leq \|\mathbf{\Pi}_M \mathbf{A}\|_2 \quad \|(I - \mathbf{\Pi}_M) \mathbf{A}\|_2 \leq \|(I - \mathbf{\Pi}_N) \mathbf{A}\|_2 \quad (9)$$

**Theorem 1** (Gap-dependent). Let  $\mathbf{\Omega} \in \mathbb{R}^{n \times \ell}$  be a standard Gaussian matrix, such that (8) holds and let  $p \geq 0$  and  $\ell \leq \min\{m, n\}$ . The outputs of Algorithm 2 satisfy the following error bound

$$\left\| \mathbf{A} - \mathbf{Q} \mathbf{Q}^\top \mathbf{S} \mathbf{A} \right\|_{T \rightarrow S}^2 \leq \|\mathbf{\Sigma}_\perp\|_2^2 + \gamma_k^{4q} \|\mathbf{\Sigma}_\perp \hat{\mathbf{\Omega}}_2 \hat{\mathbf{\Omega}}_1^\dagger\|_2^2.$$

*Proof.* There are three main steps in this proof, which heavily relies on the proof technique of [7, Theorem 9.1]. However, we need to pay close attention to the weighted inner products.

#### Step 1. Converting to standard norms

Using the property of the  $\|\cdot\|_{T \rightarrow S}$  norms

$$\left\| (I - \mathbf{Q} \mathbf{Q}^\top \mathbf{S}) \mathbf{A} \right\|_{T \rightarrow S} = \|\mathbf{S}^{1/2} (I - \mathbf{Q} \mathbf{Q}^\top \mathbf{S}) \mathbf{A} \mathbf{T}^{-1/2}\|_2.$$

Plugging in the generalized SVD of  $\mathbf{A}$ , we have

$$\begin{aligned} \mathbf{S}^{1/2}(\mathbf{I} - \mathbf{Q}\mathbf{Q}^\top \mathbf{S})\mathbf{A}\mathbf{T}^{-1/2} &= \mathbf{S}^{1/2}(\mathbf{I} - \mathbf{Q}\mathbf{Q}^\top \mathbf{S})\mathbf{U}\mathbf{\Sigma}\mathbf{V}^\top \mathbf{T}\mathbf{T}^{-1/2} \\ &= \mathbf{S}^{1/2}(\mathbf{U} - \mathbf{Q}\mathbf{Q}^\top \mathbf{S}\mathbf{U})\mathbf{\Sigma}\mathbf{V}^\top \mathbf{T}^{1/2} \\ &= \mathbf{S}^{1/2}\mathbf{U}(\mathbf{I} - \mathbf{U}^\top \mathbf{S}\mathbf{Q}\mathbf{Q}^\top \mathbf{S}\mathbf{U})\mathbf{\Sigma}\mathbf{V}^\top \mathbf{T}^{1/2} \quad (\text{since } \mathbf{U}\mathbf{U}^\top \mathbf{S} = \mathbf{I}) \\ &= \mathbf{S}^{1/2}\mathbf{U}(\mathbf{I} - \mathbf{\Pi}_{\mathbf{U}^\top \mathbf{S}\mathbf{Q}})\mathbf{\Sigma}\mathbf{V}^\top \mathbf{T}^{1/2}. \end{aligned}$$

In the last step, we have used the fact that  $\mathbf{U}^\top \mathbf{S}\mathbf{Q}$  has orthonormal columns. Combining the intermediate steps we have

$$\begin{aligned} \left\| (\mathbf{I} - \mathbf{Q}\mathbf{Q}^\top \mathbf{S})\mathbf{A} \right\|_{\mathbf{T} \rightarrow \mathbf{S}} &= \left\| \mathbf{S}^{1/2}(\mathbf{I} - \mathbf{Q}\mathbf{Q}^\top \mathbf{S})\mathbf{A}\mathbf{T}^{-1/2} \right\|_2 \\ &= \left\| \mathbf{S}^{1/2}\mathbf{U}(\mathbf{I} - \mathbf{\Pi}_{\mathbf{U}^\top \mathbf{S}\mathbf{Q}})\mathbf{\Sigma}\mathbf{V}^\top \mathbf{T}^{1/2} \right\|_2 = \left\| (\mathbf{I} - \mathbf{\Pi}_{\mathbf{U}^\top \mathbf{S}\mathbf{Q}})\mathbf{\Sigma} \right\|_2, \end{aligned}$$

In the last step, we have used the fact that  $\mathbf{S}^{1/2}\mathbf{U}$  and  $\mathbf{T}^{1/2}\mathbf{V}$  are orthogonal matrices, and that the spectral norm is unitarily invariant.

## Step 2. Reducing dimension from $\ell$ to $k$

From the generalized SVD of  $\mathbf{A}$

$$\mathbf{U}^\top \mathbf{S}\mathbf{Y} = \mathbf{U}^\top \mathbf{S}\mathbf{U}(\mathbf{\Sigma}\mathbf{\Sigma}^\top)^q \mathbf{\Sigma}\mathbf{V}^\top \mathbf{T}\mathbf{\Omega} = \begin{bmatrix} \mathbf{\Sigma}_k^{2q+1} \hat{\mathbf{\Omega}}_1 \\ (\mathbf{\Sigma}_\perp \mathbf{\Sigma}_\perp^\top)^q \mathbf{\Sigma}_\perp \hat{\mathbf{\Omega}}_2 \end{bmatrix}.$$

By assumption,  $\hat{\mathbf{\Omega}}_1$  has a right multiplicative inverse and define

$$\mathbf{Z} \equiv \mathbf{U}^\top \mathbf{S}\mathbf{Y} \hat{\mathbf{\Omega}}_1^\dagger \mathbf{\Sigma}_k^{-(2q+1)} = \begin{bmatrix} \mathbf{I} \\ \mathbf{F} \end{bmatrix}, \quad \text{where } \mathbf{F} \equiv (\mathbf{\Sigma}_\perp \mathbf{\Sigma}_\perp^\top)^q \mathbf{\Sigma}_\perp \hat{\mathbf{\Omega}}_2 \hat{\mathbf{\Omega}}_1^\dagger \mathbf{\Sigma}_k^{-(2q+1)}.$$

From the above equation, we have  $\text{range}(\mathbf{Z}) \subset \text{range}(\mathbf{U}^\top \mathbf{S}\mathbf{Y}) \subset \text{range}(\mathbf{U}^\top \mathbf{S}\mathbf{Q})$ . Therefore,

$$\mathbf{\Pi}_Z \leq \mathbf{\Pi}_{\mathbf{U}^\top \mathbf{S}\mathbf{Q}} \quad \mathbf{I} - \mathbf{\Pi}_{\mathbf{U}^\top \mathbf{S}\mathbf{Q}} \leq \mathbf{I} - \mathbf{\Pi}_Z.$$

This step has reduced the dimensionality from an  $\ell = k + p$  dimensional space to a  $k$  dimensional space, since the number of columns of  $\mathbf{Z}$  is  $k$ .

## Step 3. Extracting diagonal subblocks

Using Eq. (9) and properties of the  $\|\cdot\|_2$  norm, we can write

$$\left\| \mathbf{A} - \mathbf{Q}\mathbf{Q}^\top \mathbf{S}\mathbf{A} \right\|_{\mathbf{T} \rightarrow \mathbf{S}}^2 = \left\| (\mathbf{I} - \mathbf{\Pi}_{\mathbf{U}^\top \mathbf{S}\mathbf{Q}})\mathbf{\Sigma} \right\|_2^2 \leq \left\| \mathbf{\Sigma}^\top (\mathbf{I} - \mathbf{\Pi}_Z)\mathbf{\Sigma} \right\|_2.$$

Next, using the definition of the spectral projector

$$\mathbf{\Pi}_Z = \begin{bmatrix} \mathbf{I} \\ \mathbf{F} \end{bmatrix} (\mathbf{F}^\top \mathbf{F} + \mathbf{I})^{-1} \begin{bmatrix} \mathbf{I} & \mathbf{F}^\top \end{bmatrix},$$

and

$$\mathbf{\Sigma}^\top (\mathbf{I} - \mathbf{\Pi}_Z)\mathbf{\Sigma} = \begin{bmatrix} \mathbf{\Sigma}_k^\top \mathbf{F}_1 \mathbf{\Sigma}_k & * \\ * & \mathbf{\Sigma}_\perp^\top \mathbf{F}_2 \mathbf{\Sigma}_\perp \end{bmatrix}$$

where  $\mathbf{F}_1 = (\mathbf{I} - (\mathbf{I} + \mathbf{F}^\top \mathbf{F})^{-1})$ ,  $\mathbf{F}_2 = (\mathbf{I} - \mathbf{F}(\mathbf{I} + \mathbf{F}^\top \mathbf{F})^{-1})\mathbf{F}^\top$  and  $*$  denote blocks that do not affect the calculations. Applying [7, Proposition 3], we obtain

$$\left\| \mathbf{\Sigma}^\top (\mathbf{I} - \mathbf{\Pi}_Z)\mathbf{\Sigma} \right\|_2 \leq \left\| \mathbf{\Sigma}_k^\top \mathbf{F}_1 \mathbf{\Sigma}_k \right\|_2 + \left\| \mathbf{\Sigma}_\perp^\top \mathbf{F}_2 \mathbf{\Sigma}_\perp \right\|_2.$$

Following the proof of [7],  $\mathbf{F}_1 \leq \mathbf{F}^\top \mathbf{F}$  and  $\mathbf{F}_2 \leq \mathbf{I}$ , so that

$$\left\| \mathbf{\Sigma}^\top (\mathbf{I} - \mathbf{\Pi}_Z)\mathbf{\Sigma} \right\|_2 \leq \left\| \mathbf{\Sigma}_k^\top \mathbf{F}^\top \mathbf{F} \mathbf{\Sigma}_k \right\|_2 + \left\| \mathbf{\Sigma}_\perp^\top \mathbf{\Sigma}_\perp \right\|_2 = \left\| \mathbf{F} \mathbf{\Sigma}_k \right\|_2^2 + \left\| \mathbf{\Sigma}_\perp \right\|_2^2. \quad (10)$$

With repeated use of the submultiplicativity inequality, we obtain  $\left\| \mathbf{F} \mathbf{\Sigma}_k \right\|_2 \leq \gamma_k^{2q} \left\| \mathbf{\Sigma}_\perp \hat{\mathbf{\Omega}}_2 \hat{\mathbf{\Omega}}_1^\dagger \right\|_2$ . Therefore,

$$\left\| (\mathbf{I} - \mathbf{\Pi}_{\mathbf{U}^\top \mathbf{S}\mathbf{Q}})\mathbf{\Sigma} \right\|_2^2 \leq \left\| \mathbf{\Sigma}_\perp \right\|_2^2 + \gamma_k^{4q} \left\| \mathbf{\Sigma}_\perp \hat{\mathbf{\Omega}}_2 \hat{\mathbf{\Omega}}_1^\dagger \right\|_2^2.$$

Combined with the result of step 1, we have the desired result.  $\square$

The following bound quantifies the accuracy of the low-rank approximation and shows but does not explicitly depend on the singular value ratio  $\gamma_k$ .

**Theorem 2** (Gap-independent bound). Assume the same setup as of Theorem 1 and let  $q \geq 0$  be the number of subspace iterations. If  $\mathbf{Q}$  is the output of Algorithm 2, then

$$\left\| \mathbf{A} - \mathbf{Q}\mathbf{Q}^\top \mathbf{S}\mathbf{A} \right\|_{T \rightarrow S} \leq \left( 1 + \|\widehat{\mathbf{\Omega}}_2 \widehat{\mathbf{\Omega}}_1^\dagger\|_2^2 \right)^{1/(4q+2)} \sigma_{k+1}.$$

*Proof.* As in the proof of Theorem 1, if  $\widehat{\mathbf{A}} = \mathbf{S}^{1/2} \mathbf{A} \mathbf{T}^{-1/2}$

$$\left\| \mathbf{A} - \mathbf{Q}\mathbf{Q}^\top \mathbf{S}\mathbf{A} \right\|_{T \rightarrow S} = \left\| (\mathbf{I} - \mathbf{\Pi}_{\mathbf{S}^{1/2}\mathbf{Q}}) \widehat{\mathbf{A}} \right\|_2.$$

We recall [7, Proposition 8.6] which says if  $\mathbf{\Pi}$  is an orthogonal projector, then for  $q \geq 0$

$$\|\mathbf{\Pi}\mathbf{M}\|_2 \leq \|\mathbf{\Pi}(\mathbf{M}\mathbf{M}^\top)^q \mathbf{M}\|_2^{1/(2q+1)}.$$

Applying the above result with  $\mathbf{\Pi} = \mathbf{I} - \mathbf{\Pi}_{\mathbf{S}^{1/2}\mathbf{Q}}$  and  $\mathbf{M} = \widehat{\mathbf{A}}$ , we have

$$\begin{aligned} \left\| (\mathbf{I} - \mathbf{\Pi}_{\mathbf{S}^{1/2}\mathbf{Q}}) \widehat{\mathbf{A}} \right\|_2 &\leq \left\| (\mathbf{I} - \mathbf{\Pi}_{\mathbf{S}^{1/2}\mathbf{Q}}) (\widehat{\mathbf{A}} \widehat{\mathbf{A}}^\top)^q \widehat{\mathbf{A}} \right\|_2^{1/(2q+1)} \\ &= \left\| (\mathbf{I} - \mathbf{\Pi}_{\mathbf{S}^{1/2}\mathbf{Q}}) \mathbf{S}^{1/2} \mathbf{B} \mathbf{T}^{-1/2} \right\|_2^{1/(2q+1)} \\ &= \left\| \mathbf{S}^{1/2} (\mathbf{I} - \mathbf{Q}\mathbf{Q}^\top \mathbf{S}) \mathbf{B} \mathbf{T}^{-1/2} \right\|_2^{1/(2q+1)} \\ &= \left\| (\mathbf{I} - \mathbf{\Pi}_{\mathbf{Q}}) \mathbf{B} \right\|_{T \rightarrow S}^{1/(2q+1)}, \end{aligned}$$

where  $\mathbf{B} = (\mathbf{A} \mathbf{T}^{-1} \mathbf{A}^\top \mathbf{S})^q \mathbf{A}$ . Using the GSVD of  $\mathbf{A}$ , we can see that  $\mathbf{B}$  has the GSVD

$$\mathbf{B} = \mathbf{U}(\mathbf{\Sigma}\mathbf{\Sigma}^\top)^q \mathbf{\Sigma} \mathbf{V}^\top \mathbf{T}.$$

Following the steps of the proof of Theorem 1, we can see that

$$\left\| (\mathbf{I} - \mathbf{\Pi}_{\mathbf{Q}}) \mathbf{B} \right\|_{T \rightarrow S} \leq \left( 1 + \|\widehat{\mathbf{\Omega}}_2 \widehat{\mathbf{\Omega}}_1^\dagger\|_2^2 \right)^{1/2} \left\| (\mathbf{\Sigma}_\perp \mathbf{\Sigma}_\perp^\top)^q \mathbf{\Sigma}_\perp \right\|_2,$$

where, as before,  $\widehat{\mathbf{\Omega}}_2 = \mathbf{V}_\perp^\top \mathbf{T} \mathbf{\Omega}$  and  $\widehat{\mathbf{\Omega}}_1 = \mathbf{V}_k^\top \mathbf{T} \mathbf{\Omega}$ . Since  $\left\| (\mathbf{\Sigma}_\perp \mathbf{\Sigma}_\perp^\top)^q \mathbf{\Sigma}_\perp \right\|_2 = \sigma_{k+1}^{2q+1}$ , we therefore have the inequalities

$$\left\| \mathbf{A} - \mathbf{Q}\mathbf{Q}^\top \mathbf{S}\mathbf{A} \right\|_{T \rightarrow S} \leq \left\| (\mathbf{I} - \mathbf{\Pi}_{\mathbf{Q}}) \mathbf{B} \right\|_{T \rightarrow S}^{1/(2q+1)} \leq \left( 1 + \|\widehat{\mathbf{\Omega}}_2 \widehat{\mathbf{\Omega}}_1^\dagger\|_2^2 \right)^{1/(4q+2)} \sigma_{k+1}.$$

□

## 4.2 | Probabilistic analysis

Thus far, we have not discussed specific choices for the distribution of the random matrix  $\mathbf{\Omega} \in \mathbb{R}^{n \times \ell}$ . In this subsection, we take  $\mathbf{\Omega}$  to a standard Gaussian random matrix and derive probabilistic results on the accuracy of the low-rank decompositions. We recall some useful facts about the extreme singular values of standard Gaussian random matrices.

**Lemma 1.** Facts about Gaussian random matrices:

1. Let  $\mathbf{G}_1 \in \mathbb{R}^{m \times n}$  be a standard Gaussian random matrix. Then

$$\mathbb{P} \left\{ \|\mathbf{G}_1\|_2 \geq \sqrt{m} + \sqrt{n} + t \right\} \leq e^{-t^2/2}.$$

2. Let  $\mathbf{G}_2 \in \mathbb{R}^{\ell \times k}$  be a standard Gaussian random matrix with  $\ell - k \geq 2$ . Then

$$\mathbb{P} \left\{ \|\mathbf{G}_2^\dagger\|_2 > t \right\} \leq \sqrt{\frac{1}{2\pi(p+1)}} \left( \frac{e\sqrt{\ell}}{p+1} \right)^{p+1} t^{-(p+1)}.$$

*Proof.* Consider the function  $f(\mathbf{G}) = \|\mathbf{G}\|_2$  which has the Lipschitz constant 1, since by the reverse triangle inequality  $|f(\mathbf{X}) - f(\mathbf{Y})| \leq \|\mathbf{X} - \mathbf{Y}\|_2 \leq \|\mathbf{X} - \mathbf{Y}\|_F$ . By [23, Theorem 5.32],  $\mathbb{E} f(\mathbf{G}_1) \leq \sqrt{m} + \sqrt{n}$ . Therefore, the result of part 1 follows from [7, Proposition 10.3]. The proof of part 2 is an application of [7, Proposition A.3]. □

Theorems 1 and 2 both identify the term  $\|\widehat{\mathbf{\Omega}}_2 \widehat{\mathbf{\Omega}}_1^\dagger\|_2$  appearing in the error bounds. Lemma 2 (see below) provides a probabilistic bound for this term when the matrix  $\mathbf{\Omega}$  is a standard Gaussian random matrix. Here, we provide an interpretation for this term. To simplify matters take  $\mathbf{T} = \mathbf{I}$ . Then, by [26, Table 1]  $\|\widehat{\mathbf{\Omega}}_2 \widehat{\mathbf{\Omega}}_1^\dagger\|_2$  is the tangent of the largest canonical angle between the subspaces spanned by the columns of (a) the random matrix  $\mathbf{\Omega}$ , and (b) the right singular vectors  $\mathbf{V}_k$ . Therefore, this term informally represents the degree of alignment between these two subspaces—in the ideal case, both the subspaces are aligned, so that this term is zero, whereas in the worst case, the two subspaces are orthogonal to each other. When  $\mathbf{T} \neq \mathbf{I}$ , this interpretation has to be modified slightly; the canonical angles are now with respect to the  $\langle \cdot, \cdot \rangle_{\mathbf{T}}$  inner products rather than the standard Euclidean inner product [11, Theorem 4.2].

Before we state and prove Lemma 2, define the matrices

$$\mathbf{\Gamma}_1 \equiv \mathbf{V}_k^\top \mathbf{T}^2 \mathbf{V}_k \in \mathbb{R}^{k \times k} \quad \mathbf{\Gamma}_2 \equiv \mathbf{V}_\perp^\top \mathbf{T}^2 \mathbf{V}_\perp \in \mathbb{R}^{(n-k) \times (n-k)}. \quad (11)$$

and the constant

$$C_g \equiv \frac{e\sqrt{\ell}}{p} \left( \frac{2/\delta}{\sqrt{2\pi(p+1)}} \right)^{1/(p+1)} \left( \sqrt{n-k} + \sqrt{\ell} + \sqrt{2 \log \frac{2}{\delta}} \right). \quad (12)$$

Observe that  $\mathbf{\Gamma}_1$  and  $\mathbf{\Gamma}_2$  are positive definite.

**Lemma 2.** Consider the notation and assumptions of Theorem 1. Let the oversampling parameter satisfy  $p \geq 2$  and  $\ell = k + p \leq \min\{m, n\}$ . Then with probability at least  $1 - \delta$

$$\|\widehat{\mathbf{\Omega}}_2 \widehat{\mathbf{\Omega}}_1^\dagger\|_2^2 \leq \|\mathbf{\Gamma}_2\|_2 \|\mathbf{\Gamma}_1^{-1}\|_2 C_g^2 \leq \kappa_2(\mathbf{T}) C_g^2.$$

*Proof.* Using the submultiplicativity of the spectral norm  $\|\widehat{\mathbf{\Omega}}_2 \widehat{\mathbf{\Omega}}_1^\dagger\|_2 \leq \|\widehat{\mathbf{\Omega}}_2\|_2 \|\widehat{\mathbf{\Omega}}_1^\dagger\|_2$ . We deal with each term separately.

**Step 1. Bound for  $\widehat{\mathbf{\Omega}}_2$**  First, consider  $\widehat{\mathbf{\Omega}}_2 = \mathbf{V}_\perp^\top \mathbf{T} \mathbf{\Omega}$ . Denote the columns of  $\mathbf{\Omega} = [\boldsymbol{\omega}_1 \dots \boldsymbol{\omega}_\ell]$ . Verify that the  $j$ -th column of  $\widehat{\mathbf{\Omega}}_2$  is Gaussian with zero mean and covariance  $\mathbf{\Gamma}_2 \equiv \mathbf{V}_\perp^\top \mathbf{T}^2 \mathbf{V}_\perp$ , since

$$\mathbb{E}[(\mathbf{V}_\perp^\top \mathbf{T} \boldsymbol{\omega}_j)(\mathbf{V}_\perp^\top \mathbf{T} \boldsymbol{\omega}_j)^\top] = \mathbf{V}_\perp^\top \mathbf{T} \mathbb{E}[\boldsymbol{\omega}_j \boldsymbol{\omega}_j^\top] \mathbf{T} \mathbf{V}_\perp = \mathbf{\Gamma}_2.$$

It follows that  $\mathbf{\Gamma}_2^{-1/2} \widehat{\mathbf{\Omega}}_2 \in \mathbb{R}^{(n-k) \times \ell}$  is a standard Gaussian random matrix. Applying the first part of Lemma 1 to  $\mathbf{\Gamma}_2^{-1/2} \widehat{\mathbf{\Omega}}_2$ , with  $t = \sqrt{2 \log \frac{2}{\delta}}$  we get that

$$\|\widehat{\mathbf{\Omega}}_2\|_2 \leq \|\mathbf{\Gamma}_2^{1/2}\|_2 \|\mathbf{\Gamma}_2^{-1/2} \widehat{\mathbf{\Omega}}_2\|_2 \leq \sqrt{\|\mathbf{\Gamma}_2\|_2} \left( \sqrt{n-k} + \sqrt{\ell} + \sqrt{2 \log \frac{2}{\delta}} \right),$$

holds with probability of failure at most  $\delta/2$ . Note that  $\|\mathbf{\Gamma}_2^{1/2}\|_2 = \sqrt{\|\mathbf{\Gamma}_2\|_2}$  because  $\mathbf{\Gamma}_2$  is symmetric positive definite.

**Step 2. Bound for  $\widehat{\mathbf{\Omega}}_1$**  Now, consider  $\widehat{\mathbf{\Omega}}_1 \in \mathbb{R}^{k \times \ell}$  whose columns are independent Gaussian vectors with zero mean and covariance  $\mathbf{\Gamma}_1 \equiv \mathbf{V}_k^\top \mathbf{T}^2 \mathbf{V}_k$ . So, as before,  $\mathbf{\Gamma}_1^{-1/2} \widehat{\mathbf{\Omega}}_1$  is a standard Gaussian random matrix. By Lemma 1,

$$\mathbb{P} \left\{ \|(\mathbf{\Gamma}_1^{-1/2} \widehat{\mathbf{\Omega}}_1)^\dagger\|_2 > t \right\} \leq \sqrt{\frac{1}{2\pi(p+1)}} \left( \frac{e\sqrt{\ell}}{p+1} \right)^{p+1} t^{-(p+1)}.$$

Set the right hand side to  $\delta/2$  and solve for  $t$  to obtain

$$\mathbb{P} \left\{ \|(\mathbf{\Gamma}_1^{-1/2} \widehat{\mathbf{\Omega}}_1)^\dagger\|_2 > \left( \frac{2/\delta}{\sqrt{2\pi(p+1)}} \right)^{1/(p+1)} \frac{e\sqrt{\ell}}{p+1} \right\} \leq \frac{\delta}{2}. \quad (13)$$

We now simplify  $\|(\mathbf{\Gamma}_1^{-1/2} \widehat{\mathbf{\Omega}}_1)^\dagger\|_2$ . By [2, Theorem 2.2.3] if  $\mathbf{C} \in \mathbb{R}^{m \times r}$  and  $\mathbf{D} \in \mathbb{R}^{r \times n}$  and  $\text{rank}(\mathbf{C}) = \text{rank}(\mathbf{D}) = r$ , then

$$(\mathbf{C}\mathbf{D})^\dagger = \mathbf{D}^\dagger \mathbf{C}^\dagger$$

Pick  $\mathbf{C} = \mathbf{\Gamma}_1^{-1/2}$  and  $\mathbf{D} = \widehat{\mathbf{\Omega}}_1$ . The above result applies since  $\text{rank}(\mathbf{\Gamma}_1^{-1/2}) = \text{rank}(\widehat{\mathbf{\Omega}}_1) = k$ . Therefore,

$$(\mathbf{\Gamma}_1^{-1/2} \widehat{\mathbf{\Omega}}_1)^\dagger = \widehat{\mathbf{\Omega}}_1^\dagger \mathbf{\Gamma}_1^{1/2},$$

and  $\|\widehat{\mathbf{\Omega}}_1^\dagger\|_2 \leq \|(\mathbf{\Gamma}_1^{-1/2}\widehat{\mathbf{\Omega}}_1)^\dagger\|_2\|\mathbf{\Gamma}_1^{-1/2}\|_2$ . Therefore, combining this result with Eq. (13), we get with probability of failure at most  $\delta/2$

$$\|\widehat{\mathbf{\Omega}}_1^\dagger\|_2 \leq \sqrt{\|\mathbf{\Gamma}_1^{-1}\|_2} \left( \frac{2/\delta}{\sqrt{2\pi(p+1)}} \right)^{1/(p+1)} \frac{e\sqrt{\ell}}{p+1}.$$

**Step 3. First bound** Combining the results of steps 1 and 2 and using a union bound, we have

$$\mathbb{P} \left\{ \|\widehat{\mathbf{\Omega}}_2\|_2 \|\widehat{\mathbf{\Omega}}_1^\dagger\|_2 > \sqrt{\|\mathbf{\Gamma}_2\|_2 \|\mathbf{\Gamma}_1^{-1}\|_2} C_g \right\} \leq \delta/2 + \delta/2 = \delta,$$

where  $C_g$  is defined in Eq. (12).

**Step 4. Second bound** Partition  $\mathbf{V}^\top \mathbf{T}^2 \mathbf{V}$  as

$$\mathbf{V}^\top \mathbf{T}^2 \mathbf{V} = \begin{bmatrix} \mathbf{V}_k^\top \mathbf{T}^2 \mathbf{V}_k & * \\ * & \mathbf{V}_\perp^\top \mathbf{T}^2 \mathbf{V}_\perp \end{bmatrix},$$

where \* denote terms that are unimportant in the calculation. Define  $\widehat{\mathbf{V}} \equiv \mathbf{T}^{1/2} \mathbf{V}$  and notice that  $\widehat{\mathbf{V}}$  is orthogonal. This implies  $\mathbf{V}^\top \mathbf{T}^2 \mathbf{V} = \widehat{\mathbf{V}}^\top \mathbf{T} \widehat{\mathbf{V}}$  and that, by similarity,  $\mathbf{V}^\top \mathbf{T}^2 \mathbf{V}$  and  $\mathbf{T}$  have the same eigenvalues. Let  $\mathbf{M} \in \mathbb{R}^{n \times n}$  and let  $\lambda_k(\cdot)$  denote the eigenvalues of a matrix arranged in descending order for  $k = 1, \dots, n$ . By Cauchy interlacing theorem [2, Theorem 3.2.9],

$$\lambda_k(\mathbf{T}) = \lambda_k(\mathbf{V}^\top \mathbf{T}^2 \mathbf{V}) \geq \lambda_k(\mathbf{V}_k^\top \mathbf{T}^2 \mathbf{V}_k) \geq \lambda_n(\mathbf{V}^\top \mathbf{T}^2 \mathbf{V}) = \lambda_n(\mathbf{T}).$$

Therefore,  $\lambda_k^{-1}(\mathbf{T}) \leq \lambda_k^{-1}(\mathbf{V}_k^\top \mathbf{T}^2 \mathbf{V}_k) \leq \lambda_n^{-1}(\mathbf{T})$ . Similarly, using Cauchy interlacing theorem

$$\lambda_1(\mathbf{T}) = \lambda_1(\mathbf{V}^\top \mathbf{T}^2 \mathbf{V}) \geq \lambda_1(\mathbf{V}_\perp^\top \mathbf{T}^2 \mathbf{V}_\perp) \geq \lambda_{k+1}(\mathbf{V}^\top \mathbf{T}^2 \mathbf{V}) = \lambda_{k+1}(\mathbf{T}).$$

Since  $\mathbf{\Gamma}_1$  and  $\mathbf{\Gamma}_2$  are positive definite, their singular values are their respective eigenvalues; therefore,

$$\frac{\lambda_{k+1}(\mathbf{T})}{\lambda_k(\mathbf{T})} \leq \|\mathbf{\Gamma}_2\|_2 \|\mathbf{\Gamma}_1^{-1}\|_2 = \frac{\lambda_1(\mathbf{V}_\perp^\top \mathbf{T}^2 \mathbf{V}_\perp)}{\lambda_k(\mathbf{V}_k^\top \mathbf{T}^2 \mathbf{V}_k)} \leq \frac{\lambda_1(\mathbf{T})}{\lambda_n(\mathbf{T})} = \kappa_2(\mathbf{T}).$$

Combine with the result of step 3, we obtain the second bound □

The proof identifies that the condition number  $\kappa_2(\mathbf{T})$  plays a role in the error analysis, which suggests that a large condition number can result in a large error. However, this may be pessimistic for the following reason. The proof also gives a lower bound  $\lambda_{k+1}(\mathbf{T})/\lambda_k(\mathbf{T})$  which can be attained by a specific instance of  $\mathbf{V}$ . This lower bound shows that an ill-conditioned matrix  $\mathbf{T}$  does not necessarily amplify the error in the low-rank approximation.

We can prove the following probabilistic bound for the error in the low-rank approximation.

**Theorem 3.** Let  $\mathbf{\Omega} \in \mathbb{R}^{n \times \ell}$  be a standard Gaussian random matrix where  $k \leq \text{rank}(\mathbf{A})$  is the target rank. Let the oversampling parameter  $p$  satisfy  $p \geq 2$ ,  $\ell = k + p \leq \min\{m, n\}$ , and the failure rate  $0 < \delta < 1$ . Let  $\mathbf{Q}$  be computed using Algorithm 2 with  $q \geq 0$  subspace iterations. With probability at least  $1 - \delta$

$$\|\mathbf{A} - \mathbf{Q}\mathbf{Q}^\top \mathbf{S}\mathbf{A}\|_{T \rightarrow S} \leq \left(1 + \gamma_k^{4q+2} \kappa_2(\mathbf{T}) C_g^2\right)^{1/2} \sigma_{k+1},$$

and

$$\|\mathbf{A} - \mathbf{Q}\mathbf{Q}^\top \mathbf{S}\mathbf{A}\|_{T \rightarrow S} \leq \left(1 + \kappa_2(\mathbf{T}) C_g^2\right)^{1/(4q+2)} \sigma_{k+1},$$

where the constant  $C_g$  is defined in (12).

*Proof.* Plug the results of Lemma 2 into the statement of Theorems 1 and 2 give the desired results. □

We make several remarks. First, if the matrix  $\mathbf{A}$  has rank- $k$ , then with high probability we recover the exact rank- $k$  generalized SVD since  $\sigma_{k+1} = 0$ . Second, the bounds depend on the condition number of the weighting matrix  $\kappa_2(\mathbf{T})$ . Third, the value of the constant  $C_g$  is likely to be not optimal and it may be possible to improve upon. It is easily seen that as  $q \rightarrow \infty$ , the factor  $\left(1 + \kappa_2(\mathbf{T}) C_g^2\right)^{1/(4q+2)}$  approaches 1 and

$$\|\mathbf{A} - \mathbf{Q}\mathbf{Q}^\top \mathbf{S}\mathbf{A}\|_{T \rightarrow S} \approx \sigma_{k+1}.$$

Similarly, if  $\gamma_k < 1$ , then  $\gamma_k^{4q}$  approaches 0, so that once again the above approximation holds.

### 4.3 | Using a preconditioner for improved accuracy

From the error analysis in Theorems 1 and 2, we see that the error bounds have the factor of  $\kappa_2(\mathbf{T})$ , which can be large if  $\mathbf{T}$  is ill-conditioned. Motivated by this observation, we propose a new choice of the distribution of  $\mathbf{\Omega}$  to mitigate the issue due to ill-conditioning.

Assume that we have an approximate factorization of the form  $\mathbf{T}^{-1} \approx \mathbf{L}\mathbf{L}^\top$ , so that we call  $\mathbf{L}$  the preconditioner of  $\mathbf{T}$ . We have two requirements of the preconditioner: (1) the condition number  $\kappa_2(\mathbf{L}^\top\mathbf{T}\mathbf{L})$  should be small compared to the condition number  $\kappa_2(\mathbf{T})$ , and (2) the operation  $\mathbf{L}^{-1}\mathbf{x}$  should be cheap to perform. For example, such a factorization may be available using the Incomplete Cholesky factorization or the Sparse Approximate Inverse preconditioner (SPAI) approach [15].

If such a preconditioner is available, we show how to improve the accuracy of the randomized algorithm for GSVD. The main idea is to sample from a different distribution to construct the matrix  $\mathbf{\Omega}$ . Let  $\{\omega_j\}_{j=1}^\ell$  be independent samples drawn from  $\mathcal{N}(\mathbf{0}, \mathbf{L}\mathbf{L}^\top)$  and let

$$\mathbf{\Omega} = [\omega_1 \dots \omega_\ell] \in \mathbb{R}^{n \times \ell}.$$

Note that we can write  $\mathbf{\Omega} = \mathbf{L}\mathbf{G}$ , where  $\mathbf{G} \in \mathbb{R}^{n \times \ell}$  is a standard Gaussian random matrix. To see this, let  $\mathbf{g}_j$  be the  $j$ -th column of  $\mathbf{G}$ . Then,  $\mathbb{E}[\omega_j] = \mathbf{0}$  and

$$\mathbb{E}[\omega_j \omega_j^\top] = \mathbf{L}\mathbb{E}[\mathbf{g}_j \mathbf{g}_j^\top] \mathbf{L}^\top = \mathbf{L}\mathbf{L}^\top.$$

We invoke Algorithm 3 with the matrix  $\mathbf{\Omega}$  constructed as before, which we call the preconditioned Gaussian random matrix. The only addition to the computational cost in Algorithm 3 is  $\ell$  additional solves involving  $\mathbf{L}$ . The following result captures the error in the low-rank approximation.

**Theorem 4** (Preconditioned Gaussian random matrix). Let  $\mathbf{\Omega} = \mathbf{L}\mathbf{G} \in \mathbb{R}^{n \times \ell}$ , where  $\mathbf{G}$  is a standard Gaussian random matrix. Consider the same assumptions and notation as of Theorem 3. With probability at least  $1 - \delta$

$$\left\| \mathbf{A} - \mathbf{Q}\mathbf{Q}^\top \mathbf{S}\mathbf{A} \right\|_{T \rightarrow S} \leq \left( 1 + \gamma_k^{4q+2} \kappa_2(\mathbf{L}^\top\mathbf{T}\mathbf{L}) C_g^2 \right)^{1/2} \sigma_{k+1},$$

and

$$\left\| \mathbf{A} - \mathbf{Q}\mathbf{Q}^\top \mathbf{S}\mathbf{A} \right\|_{T \rightarrow S} \leq \left( 1 + \kappa_2(\mathbf{L}^\top\mathbf{T}\mathbf{L}) C_g^2 \right)^{1/(4q+2)} \sigma_{k+1},$$

where the constant  $C_g$  is defined in Eq. (12).

*Proof.* From Theorems 1 and 2, it is clear that we have to focus on  $\|\widehat{\mathbf{\Omega}}_2 \widehat{\mathbf{\Omega}}_1^\dagger\|_2$  which appears in the statement of both theorems. Now define  $\mathbf{Y} \equiv \mathbf{T}\mathbf{L}\mathbf{L}^\top\mathbf{T}$  and in analogy with (11) define

$$\mathbf{\Gamma}_2 \equiv \mathbf{V}_\perp^\top \mathbf{Y} \mathbf{V}_\perp \quad \mathbf{\Gamma}_1 \equiv \mathbf{V}_k^\top \mathbf{Y} \mathbf{V}_k.$$

Verify that  $\mathbf{\Gamma}_2^{-1/2} \widehat{\mathbf{\Omega}}_2 \in \mathbb{R}^{(n-k) \times \ell}$  and  $\mathbf{\Gamma}_1^{-1/2} \widehat{\mathbf{\Omega}}_1 \in \mathbb{R}^{k \times \ell}$  are both standard Gaussian random matrices. Therefore, combining steps 1 to 3 of the proof of Lemma 2, with probability at least  $1 - \delta$

$$\|\widehat{\mathbf{\Omega}}_2 \widehat{\mathbf{\Omega}}_1^\dagger\|_2 \leq \|\mathbf{\Gamma}_2\|_2 \|\mathbf{\Gamma}_1^{-1}\|_2 C_g^2.$$

Note that  $\mathbf{V}^\top \mathbf{Y} \mathbf{V} = \mathbf{V}^\top \mathbf{T}^{1/2} \mathbf{T}^{1/2} (\mathbf{L}\mathbf{L}^\top) \mathbf{T}^{1/2} \mathbf{T}^{1/2} \mathbf{V}$ . Since  $\mathbf{T}^{1/2} \mathbf{V}$  is orthogonal,  $\mathbf{V}^\top \mathbf{Y} \mathbf{V}$  and  $\mathbf{T}^{1/2} (\mathbf{L}\mathbf{L}^\top) \mathbf{T}^{1/2}$  have the same eigenvalues. By Cauchy interlacing theorem, we have

$$\|\mathbf{\Gamma}_2\|_2 \|\mathbf{\Gamma}_1^{-1}\|_2 = \frac{\lambda_1(\mathbf{V}_\perp^\top \mathbf{Y} \mathbf{V}_\perp)}{\lambda_k(\mathbf{V}_k^\top \mathbf{Y} \mathbf{V}_k)} \leq \frac{\lambda_1(\mathbf{T}^{1/2} (\mathbf{L}\mathbf{L}^\top) \mathbf{T}^{1/2})}{\lambda_n(\mathbf{T}^{1/2} (\mathbf{L}\mathbf{L}^\top) \mathbf{T}^{1/2})}.$$

If  $\mathbf{C}, \mathbf{D} \in \mathbb{R}^{n \times n}$  then  $\mathbf{C}\mathbf{D}$  and  $\mathbf{D}\mathbf{C}$  have the same eigenvalues; see [10, Theorem 1.3.22]; so,  $\mathbf{T}^{1/2} (\mathbf{L}\mathbf{L}^\top) \mathbf{T}^{1/2}$  has the same eigenvalues as  $\mathbf{L}^\top \mathbf{T} \mathbf{L}$ . Therefore, with probability at least  $1 - \delta$

$$\|\widehat{\mathbf{\Omega}}_2 \widehat{\mathbf{\Omega}}_1^\dagger\|_2^2 \leq \|\mathbf{\Gamma}_2\|_2 \|\mathbf{\Gamma}_1^{-1}\|_2 C_g^2 \leq \kappa_2(\mathbf{L}^\top \mathbf{T} \mathbf{L}) C_g^2.$$

Plug this bound into the results of Theorems 1 and 2 to obtain the desired result.  $\square$

If the preconditioned operator  $\mathbf{L}^\top \mathbf{T} \mathbf{L}$  has a lower condition number than  $\mathbf{T}$ , then the bound in Theorem 4 suggests that the error should be lower (this is confirmed by numerical experiments). Of course, from an accuracy perspective, in the ideal case  $\mathbf{L} = \mathbf{T}^{-1/2}$  so that the preconditioned operator has a condition number of 1.

#### 4.4 | Analysis of randomized algorithm for GHEP

Consider the GHEP

$$\mathbf{A}\mathbf{x} = \lambda\mathbf{B}\mathbf{x}, \quad (14)$$

where  $\mathbf{A}, \mathbf{B} \in \mathbb{R}^{n \times n}$  are symmetric,  $\mathbf{A}$  is positive semidefinite, and  $\mathbf{B}$  is positive definite. We can extend the analysis developed in this section to a randomized algorithm for GHEP.

To this end, consider the generalized eigenvalues of Eq. (14) in descending order

$$\lambda_1 \geq \dots \geq \lambda_k \geq \lambda_{k+1} \geq \dots \geq \lambda_n.$$

Let us define  $\mathbf{C} \equiv \mathbf{B}^{-1}\mathbf{A}$ ; note that  $\lambda_j$ 's are also the eigenvalues of  $\mathbf{C}$ . Furthermore observe that the  $(\mathbf{B}, \mathbf{B})$ -generalized singular values of  $\mathbf{C}$  satisfy for  $j = 1, \dots, n$

$$\sigma_j(\mathbf{C}) = s_j(\mathbf{B}^{1/2}\mathbf{C}\mathbf{B}^{-1/2}) = s_j(\mathbf{B}^{-1/2}\mathbf{A}\mathbf{B}^{-1/2}) = \lambda_j.$$

As before, we draw a Gaussian random matrix  $\mathbf{\Omega} \in \mathbb{R}^{n \times \ell}$  and form  $\mathbf{Y} = \mathbf{C}\mathbf{\Omega}$ . Then, we compute the weighted QR factorization of  $\mathbf{Y} = \mathbf{Q}\mathbf{R}$  where  $\mathbf{Q}$  has  $\mathbf{B}$ -orthonormal columns. Then, we have the low-rank approximation

$$\mathbf{C} \approx \mathbf{Q}\mathbf{Q}^\top \mathbf{B}\mathbf{C} = \mathbf{\Pi}_\mathbf{Q}\mathbf{C}.$$

To analyze the error in this low-rank representation, we can apply Theorem 3 with  $q = 0$ ,  $m = n$  and  $\mathbf{S} = \mathbf{T} = \mathbf{B}$ . As before, let  $0 < \delta < 1$  be a user-defined parameter that denotes the probability of failure. With probability at least  $1 - \delta$ ,

$$\|(\mathbf{I} - \mathbf{Q}\mathbf{Q}^\top \mathbf{B})\mathbf{C}\|_{\mathbf{B} \rightarrow \mathbf{B}} \leq \left(1 + \kappa_2(\mathbf{B})C_g^2\right)^{1/2} \lambda_{k+1}, \quad (15)$$

This bound is easy to interpret, since the absolute error is expressed in terms of the  $(k + 1)$ -th generalized eigenvalue. This provides an alternative to [18, Theorem 1]; however, a direct comparison between these two results is difficult since the results are expressed using the  $(\mathbf{B}, \mathbf{I})$ -GSVD of  $\mathbf{C}$ . We would also like to mention that the final result in [18, Theorem 1] is missing a factor of 2 on the right hand side. If a symmetric low-rank representation is desired, we can use the approximation

$$\mathbf{C} \approx \mathbf{\Pi}_\mathbf{Q}\mathbf{C}\mathbf{\Pi}_\mathbf{Q} \quad \text{or} \quad \mathbf{A} \approx \mathbf{Q}\mathbf{Q}^\top \mathbf{B}\mathbf{A}\mathbf{Q}\mathbf{Q}^\top \mathbf{B},$$

where  $\mathbf{\Pi}_\mathbf{Q} = \mathbf{Q}\mathbf{Q}^\top \mathbf{B}$ . Using [18, Equation (7)],

$$\|\mathbf{C} - \mathbf{\Pi}_\mathbf{Q}\mathbf{C}\mathbf{\Pi}_\mathbf{Q}\|_{\mathbf{B} \rightarrow \mathbf{B}} \leq 2\|\mathbf{C} - \mathbf{\Pi}_\mathbf{Q}\mathbf{C}\|_{\mathbf{B} \rightarrow \mathbf{B}}.$$

Combined with Eq. (15), we have with probability at least  $1 - \delta$

$$\|\mathbf{C} - \mathbf{\Pi}_\mathbf{Q}\mathbf{C}\mathbf{\Pi}_\mathbf{Q}\|_{\mathbf{B} \rightarrow \mathbf{B}} \leq 2\left(1 + \kappa_2(\mathbf{B})C_g^2\right)^{1/2} \lambda_{k+1}.$$

This analysis is beneficial for the computation of the GSVD which has been formulated as an appropriate GHEP as in Section 3.4. Furthermore, we note that the basic version of the algorithm can be improved by using a variation of the randomized subspace iteration, Algorithm 2. Additional theoretical results can be derived using the approach in Theorem 1 or Theorem 2.

## 5 | NUMERICAL EXPERIMENTS

In Section 5.1, we apply the proposed algorithms on a set of test matrices. The numerical experiments explore various features of the algorithms such as the number of subspace iterations and condition number of the weighting matrices. Furthermore, we compare the performance of the proposed algorithms against previously proposed algorithms. In Section 5.2, we present a numerical study of the robustness of randomized algorithms to inexactness arising in HDSA applications. Then, in Section 5.3, we apply the randomized algorithms to compute hyper-differential sensitivity indices, and demonstrate the accuracy and computational benefits of the proposed algorithms.

### 5.1 | Experiments with Test Matrices

#### 5.1.1 | Description of the test matrices

For the matrix  $\mathbf{A} \in \mathbb{R}^{128 \times 128}$ , we have the following choices:

1. **Controlled gap** The first test matrix  $\mathbf{A} \in \mathbb{R}^{128 \times 128}$  is constructed using the formula

$$\mathbf{A} = \sum_{j=1}^r \frac{\text{gap}}{j} \mathbf{x}_j \mathbf{y}_j^\top + \sum_{j=r+1}^{128} \frac{1}{j} \mathbf{x}_j \mathbf{y}_j^\top,$$

where  $\mathbf{x}_j \in \mathbb{R}^{128}$  and  $\mathbf{y}_j \in \mathbb{R}^{128}$  are sparse random vectors with non-negative entries generated using the MATLAB commands `sprand(128, 1, 0.025)` and `sprand(128, 1, 0.025)` respectively and `gap = 10`.

2. **Low-rank plus noise** which takes the form

$$\mathbf{A} = \begin{bmatrix} \mathbf{I}_r & \mathbf{0} \\ \mathbf{0} & \mathbf{0} \end{bmatrix} + \sqrt{\frac{\gamma_{\text{noise}}^r}{2n^2}} (\mathbf{G} + \mathbf{G}^\top),$$

where  $\mathbf{G} \in \mathbb{R}^{n \times n}$  is a random Gaussian matrix and we take  $\gamma_{\text{noise}} = 10^{-2}$ .

3. **Low-rank plus decay** which takes the form

$$\mathbf{A} = \text{diag}(\underbrace{1, 1, \dots, 1}_r, 2^{-d}, 3^{-d}, \dots, (n-r+1)^{-d}),$$

where  $n = 128$  and  $d = 1$ .

4. **Decay** which takes the form

$$\mathbf{A} = \text{diag}(0.9^1, \dots, 0.9^{128}).$$

The test matrices described here, model different scenarios of singular value decay. A more detailed description of these matrices is described in [16, Section 6.1]. We take the parameter  $r = 15$ . The matrices  $\mathbf{S}$  and  $\mathbf{T}$  are both generate using MATLAB's `gallery` function. The matrix  $\mathbf{S}$  is computed using `gallery('minij', 128)`, whereas  $\mathbf{T}$  is generated using `gallery('randsvd', n, -10^4, 5)` with the condition number  $10^4$ .

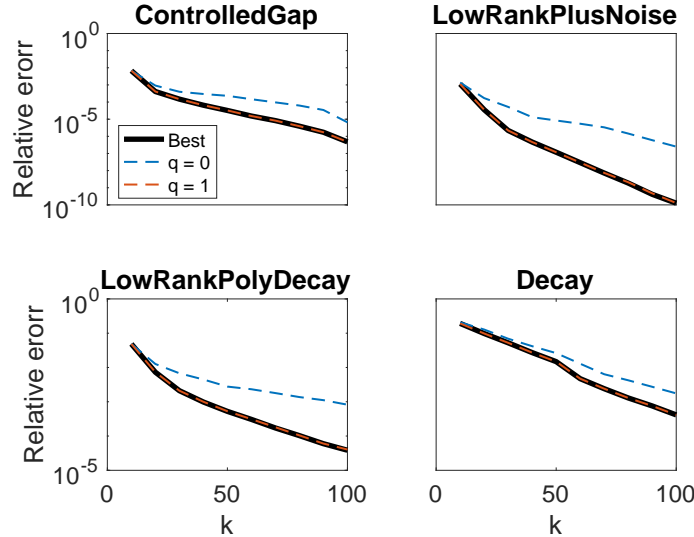


**FIGURE 1** The error in the low-rank approximations obtained using subspace iterations  $q = 0, 1$ . ‘Best’ refers to  $\sigma_{k+1}/\sigma_1$ , the error in the best rank- $k$  representation.

For each test matrix, we apply Algorithm 3, and compute a low-rank approximation as a function of the target rank  $k$ . The error in the low-rank approximation is plotted in Fig. 1. The oversampling parameter is taken to be  $p = 10$  and the number of subspace iterations  $q = 0, 1$ . If  $\hat{\mathbf{A}}$  is an approximation of  $\mathbf{A}$ , the relative error is defined as

$$\text{error} \equiv \frac{\|\mathbf{A} - \hat{\mathbf{A}}\|_{T \rightarrow S}}{\|\mathbf{A}\|_{T \rightarrow S}}.$$

For all the test matrices, we see that the error in the low-rank approximation decreases as the target rank  $k$  increases. We also observe that, with increasing subspace iterations, the error in the low-rank approximation decreases and with one subspace iteration  $q = 1$ , the error is comparable to the “best” possible error  $\sigma_{k+1}/\sigma_1$ .

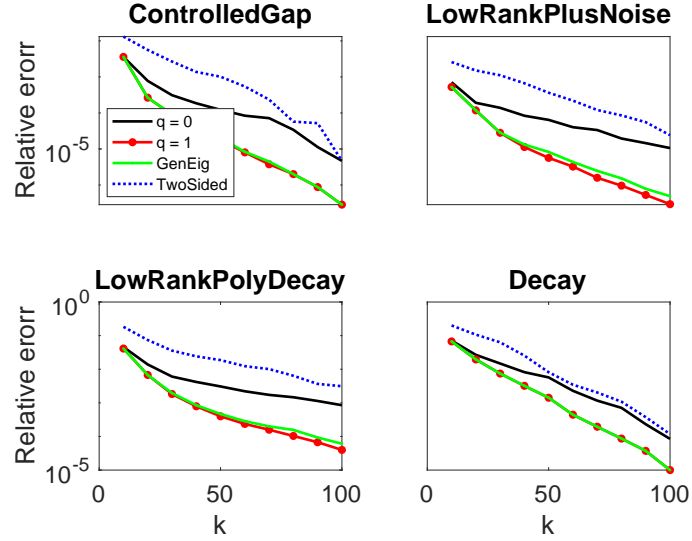


FIGURE 2 Comparing the accuracy between different methods.

### 5.1.2 | Comparing different methods

We want to compare the performance of Algorithm 3, which we call ‘GSVD( $q$ )’ where  $q$  denotes the number of subspace iteration with two other approaches. The first method computes the GSVD by formulating it as a GHEP  $\mathbf{A}^\top \mathbf{S} \mathbf{A} \mathbf{x} = \lambda \mathbf{T} \mathbf{x}$  as described in Section 3.4; we call this ‘GenEig.’ The second method, first described in [18, Section 3], uses a two-sided approach as follows. We draw two random matrices  $\mathbf{\Omega} \in \mathbb{R}^{n \times \ell}$  and  $\mathbf{\Psi} \in \mathbb{R}^{m \times \ell}$  and compute  $\mathbf{Y}_\Omega = \mathbf{A} \mathbf{\Omega}$  and  $\mathbf{Y}_\Psi = \mathbf{A}^\top \mathbf{\Psi}$ . We compute the thin QR factorization of  $\mathbf{Y}_\Omega$  and  $\mathbf{Y}_\Psi$  to obtain  $\mathbf{Q}$  (which has  $\mathbf{S}$ -orthonormal columns), and  $\mathbf{Z}$  (which has  $\mathbf{T}^{-1}$ -orthonormal columns) respectively. This results in the low-rank approximation

$$\mathbf{A} \approx \mathbf{Q} \mathbf{Q}^\top \mathbf{S} \mathbf{A} \mathbf{T}^{-1} \mathbf{Z} \mathbf{Z}^\top.$$

To convert into the GSVD format, we compute  $\mathbf{F} = \mathbf{Q}^\top \mathbf{S} \mathbf{A} \mathbf{T}^{-1} \mathbf{Z}$  and its thin SVD  $\mathbf{F} = \mathbf{U}_F \hat{\mathbf{\Sigma}} \mathbf{V}_F^\top$ . We obtain  $\mathbf{A} \approx \hat{\mathbf{U}} \hat{\mathbf{\Sigma}} \hat{\mathbf{V}}^\top$  by computing  $\hat{\mathbf{U}} = \mathbf{Q} \mathbf{U}_F$  and  $\hat{\mathbf{V}} = \mathbf{T}^{-1} \mathbf{Z} \mathbf{V}_F$  which is denoted as the ‘Two-Sided’ approach. We point out that because of a mathematical error, [18, Section 3] we do not compute the  $(\mathbf{S}, \mathbf{T})$ -GSVD of  $\mathbf{A}$ , and the procedure described above is used instead. Fig. 2 compares the error in all four test matrices described. The matrices  $\mathbf{S}$  and  $\mathbf{T}$  are defined as before. We observe that ‘GSVD(1)’ is the most accurate. However, ‘GenEig’ are computational comparable but slightly less accurate. The ‘TwoSided’ approach is more expensive and has the worst error.

Fig. 2 compares the accuracy in the low-rank approximations. We now examine the accuracy of the computed singular values and singular vectors. For our next experiment, we pick the second test matrix ‘Low-rank plus decay’ and fix  $k = 50$  and  $p = 10$ . The conclusions we describe below for this matrix are consistent with other test matrices. The left panel in Fig. 3 shows the absolute error in singular values computed using the different methods. We observe in each method that the error in the larger singular values is smaller. As before, we see that ‘TwoSided’ and Algorithm 3 with  $q = 0$  have the worst performance. Although ‘GenEig’ does far better than these two methods, Algorithm 3 with  $q = 1$  produces the most accurate singular values. Next, we compare the accuracy of the singular vectors by means of the canonical angles. Suppose  $\mathbf{Z}, \hat{\mathbf{Z}} \in \mathbb{R}^{n \times k}$  have  $\mathbf{W}$  orthonormal columns, then the cosine of the canonical angles can be computed by the singular values of  $\hat{\mathbf{Z}}^\top \mathbf{W} \mathbf{Z}$ . See [11] for definitions and details of the computation. The center panel of Fig. 3 plots the canonical angles between the “exact” and approximate left singular vectors; similarly, the right panel plots the canonical angles between the “exact” and approximate right singular vectors. For the left singular vectors, ‘TwoSided’ is comparable with ‘GSVD(0)’, whereas ‘GenEig’ is comparable with ‘GSVD(1)’. However,

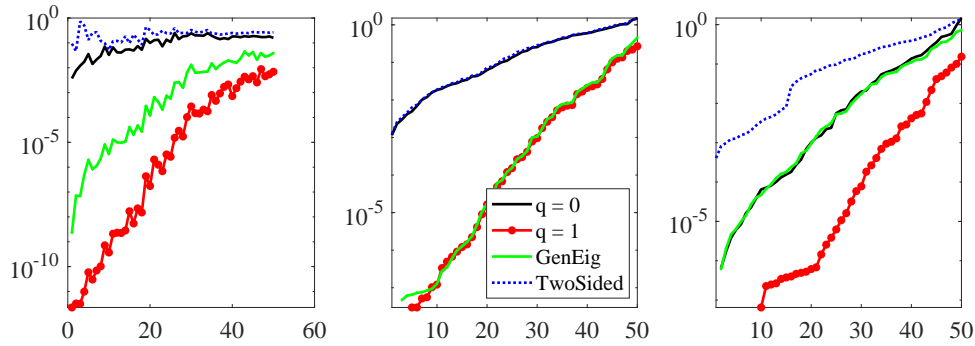


**FIGURE 3** Comparing the accuracy between different methods (left) absolute error in the singular values, (center) canonical angles between the “exact” and approximate left singular vectors, and (right) canonical angles corresponding to the right singular vectors.

for the right singular vectors, ‘GSVD(1)’ is the most accurate. The accuracy of the right singular vectors can be explained by the arguments made in [16] (see discussion after Theorem 1). While the accuracy of low-rank representations using ‘GenEig’ and ‘GSVD(1)’ is comparable, there is a considerable difference in the accuracy of the singular values and the singular vectors. For this reason, we do not use the ‘TwoSided’ in subsequent experiments.

### 5.1.3 | Effect of condition number

Section 4, and in particular Theorems 1 and 2, clearly identified the role of condition number  $\kappa_2(\mathbf{T})$  in the error analysis. We investigate the extent of the impact of a large condition number. For this purpose, we select the ‘Low-rank plus decay’ matrix and the same  $\mathbf{S}$  matrix, described in Section 5.1.1. However, we construct four different matrices for  $\mathbf{T}$  using MATLAB’s `gallery/randsvd` with condition numbers  $\{10, 10^4, 10^7, 10^{10}\}$ . The relative error in the low-rank approximation is plotted as a function of the target rank  $k$ ; the oversampling parameter is still  $p = 10$ . The results are plotting in Fig. 4. Two main observations can be drawn: first, the error appears to increase with increasing condition number, confirming the analysis, and second, subspace iteration with  $q = 1$  is sufficiently accurate to counteract the effects of ill-conditioning. We observe similar trends for other choices of  $\mathbf{A}$  but do not report them here.

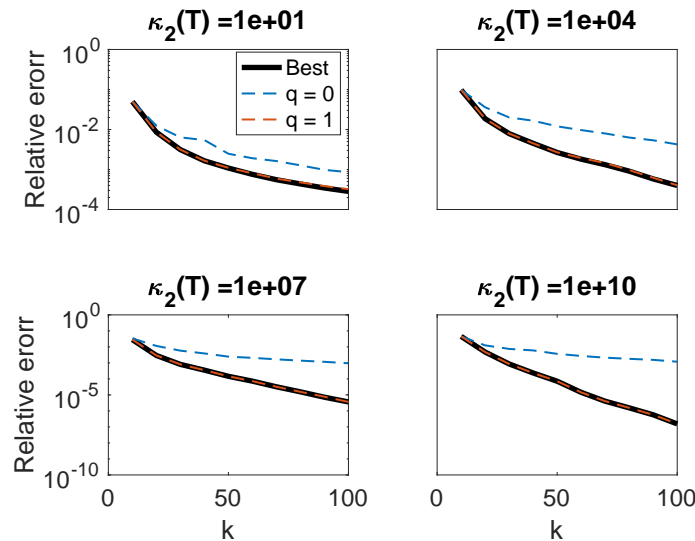


**FIGURE 4** The relative error in the low-rank representations obtained using subspace iteration with increasing condition number of  $\mathbf{T}$ . In general, a larger condition number results in a larger error confirming the analysis in Section 4.2. Here, ‘Best’ refers to the relative error in the best low-rank representation, i.e.,  $\sigma_{k+1}/\sigma_1$ .

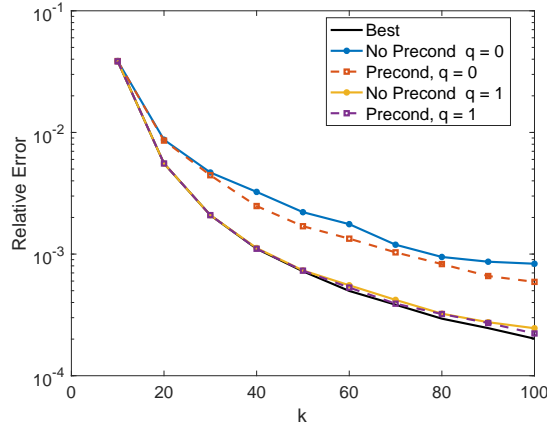


**FIGURE 5** The effect of the preconditioning on the relative error in the low-rank representation. Here, ‘Best’ refers to the relative error in the best low-rank representation, i.e.,  $\sigma_{k+1}/\sigma_1$ .

In the next experiment, we take  $T$  as the matrix HB/no7 from the SuiteSparse matrix collection [3]. This matrix is of size  $729 \times 729$  with a condition number  $\approx 2.4 \times 10^9$ . The matrices  $A$  and  $S$  are constructed in the same way as the previous experiment; the only difference is that they are both of size  $729 \times 729$ . The preconditioner is constructed using Incomplete Cholesky factorization via MATLAB’s `ichol` with drop tolerance  $10^{-4}$ , and parameter ‘michol’ set to ‘on’. The preconditioned operator has the condition number  $\kappa_2(LTL^\top) \approx 1.4 \times 10^5$ . We compute the relative error in the low-rank representations with and without preconditioner and the results are reported in Fig. 5. It is readily seen that the use of the preconditioner improves the accuracy especially for the larger values of the target rank. However, as with the previous experiment,  $q = 1$  subspace iterations is sufficient to produce an accurate low-rank representations. We conclude if  $T^{-1}$  is cheap to apply, then an additional round of subspace iteration is recommended. If, on the other hand,  $T$  is too expensive to apply, but a good preconditioner is available, it can be used to improve accuracy.

## 5.2 | Numerical Study of Inexactness in HDSA

In our next experiment, we discuss issues related to inexact matvecs in HDSA. Recall that  $A$  arises from the discretization of the operator  $Dz^* = \Pi K^{-1}B$ . The computation of a matrix-vector product  $Ax$  can be done as

$$Ax = \Pi(K^{-1}(Bx)),$$

where  $\Pi, K, B$  are discretized versions of  $\Pi, \mathcal{K}$  and  $B$  respectively. The application of the transpose of  $A$  can be performed similarly. It is clear that the dominant cost involves solving linear systems involving  $K$ , when  $K$  is large and it is natural to turn to iterative methods such as Conjugate Gradient. In this experiment, we investigate the impact of the tolerance, used as a stopping criterion in the iterative algorithm, on the accuracy of the generalized singular values obtained using the randomized algorithm. To this end, we use operators from the source inversion example in [9] (which were constructed explicitly at significant computational cost for this experiment) and use Conjugate Gradient for solving linear systems involving  $K$ . We choose three different tolerances, which controls the relative residual, for the stopping criterion  $\text{tol} \in \{10^{-3}, 10^{-6}, 10^{-9}\}$ . For comparison, we also use a direct solver. In all the experiments we have used an oversampling parameter  $p = 10$ . We see that the absolute error in the singular values is high when the tolerance is  $10^{-3}$ ; however, as the tolerance is decreased, we see that the error is almost indistinguishable from the direct solution. This is consistent with the theory and numerical experiments in [5, 25, 19] but more rigorous error analysis is needed to explore the effect of inexactness on the quality of the low-rank approximation.

## 5.3 | Application of HDSA for PDE-constrained optimal control

In this subsection we demonstrate the utility of the randomized GSVD to compute hyper-differential sensitivity indices for a PDE-constrained optimal control problem with spatially heterogeneous uncertain parameters in a model for subsurface fluid

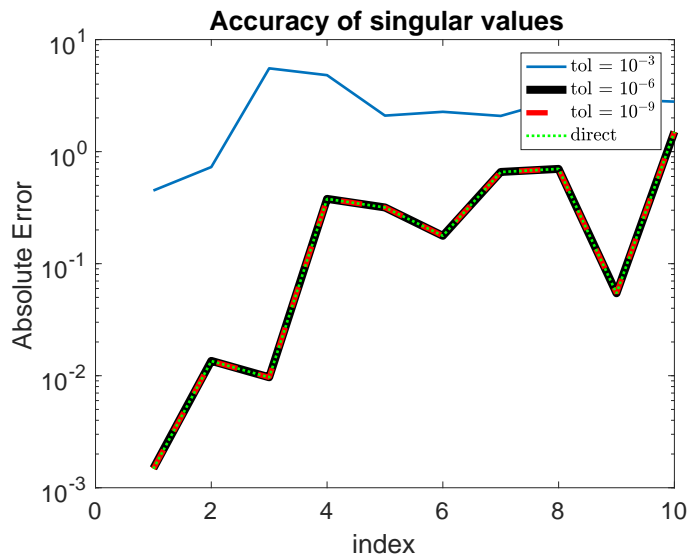


**FIGURE 6** The effect of the tolerance used in the stopping criterion on the absolute error in the singular values. The label ‘direct’ refers to using a direct solver for solving systems with  $\mathbf{K}$ .

flow. Direct computation of such sensitivity indices, in this example, would require 8,800 matvecs, whereas by using the GSVD we reduce this to 96 matvecs. This results in a dramatic computational savings since each matvec requires many PDE solves.

### Control Problem:

Consider the PDE-constrained optimal control problem

$$\min_{u,z} \frac{1}{2} \sum_{j=1}^r (\mathcal{P}_j u - T_j)^2 + \frac{\alpha}{2} \sum_{i=1}^m z_i^2 \quad (16)$$

such that

$$\begin{aligned} -\nabla \cdot (\mu \nabla u) &= \sum_{i=1}^m z_i f_i && \text{in } \Omega \\ u &= \psi && \text{on } \Gamma_D \\ -\mu \nabla u \cdot \mathbf{n} &= 0 && \text{on } \Gamma_N \end{aligned}$$

where  $\Omega = (0, 1)^3$  is the computational domain with Dirichlet boundary  $\Gamma_D = \{0\} \times (0, 1)^2 \cup \{1\} \times (0, 1)^2$  and Neumann boundary  $\Gamma_N$  given by the remaining six sides of the unit cube  $\Omega$ , i.e.  $\partial\Omega \setminus \Gamma_D$ ;  $\mathbf{n}$  denotes the outward pointing normal vector to the boundary. We use  $(x_1, x_2, x_3) \in \Omega$  to denote spatial coordinates when needed.

The PDE in (16) arises from Darcy’s law for subsurface porous media flow. It depends upon the spatially heterogeneous permeability field  $\mu$  and a source term defined by a sum of  $m$  spatially localized injections  $f_i, i = 1, 2, \dots, m$ , which are weighted by entries of the control vector  $\mathbf{z} \in \mathbb{R}^m$ . The optimal control problem seeks to determine injection magnitudes  $z_i, i = 1, 2, \dots, m$ , so that the pressure field  $u$  attains a target value  $T_j, j = 1, 2, \dots, r$ , at  $r$  different spatial coordinates,  $\mathcal{P}_j$  is the point-wise evaluation operator mapping  $u$  to its value at the  $j^{\text{th}}$  spatial coordinate.

Assuming that the permeability field  $\mu$  and Dirichlet boundary condition  $\psi$  are known, Eq. (16) may be solved using PDE-constrained optimization techniques. However,  $\mu$  and  $\psi$  are typically difficult to estimate in practice which motivates interest in the sensitivity of the optimal controller to perturbations of  $\mu$  and  $\psi$ .

Fig. 7 displays the optimal controller and a comparison of the target pressure with the controlled and uncontrolled state. The left panel displays the optimal injection magnitudes  $z_i, i = 1, 2, \dots, m$ , with their spatial location given by the position of the circle in the cube  $\Omega$  and the injection magnitude indicated by the circle’s color. The injections are permitted in sixteen predetermined wells. The right panel compares the target data, uncontrolled state, and controlled state in a  $x_1 - x_2$  cross section with  $x_3 = 0.53$  fixed. The vertical axis in this figure indicates the pressure. The sixteen cyan circles indicate the location (in the  $x_1 - x_2$  cross section) of the sixteen injection wells where the controller acts.

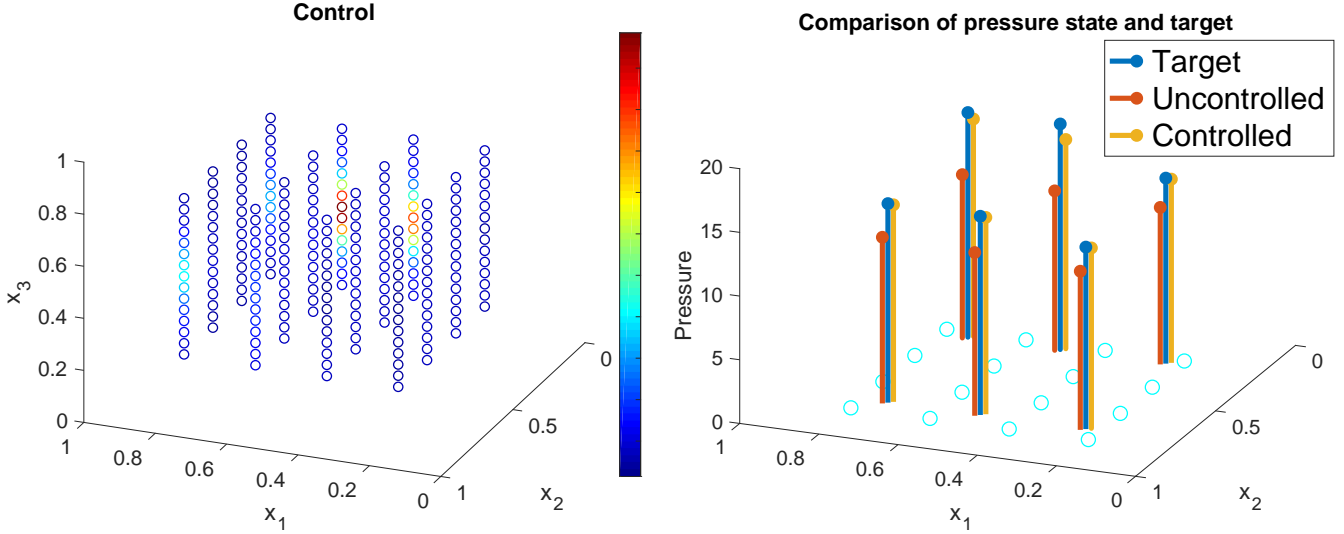


**FIGURE 7** Left: optimal control strategy (injection magnitudes) in sixteen wells; right: comparison of the target data, uncontrolled, and controlled state, the cyan circles indicate the positions of the injection wells (coinciding with the sixteen wells in the left figure).

### Parameter specification:

We represent uncertainty in the permeability field  $\mu$ , a function defined on  $\Omega$ , and Dirichlet boundary conditions  $\psi_0$  (at  $x_1 = 0$ ) and  $\psi_1$  (at  $x_1 = 1$ ), functions defined on  $\Gamma_D$ , by prescribing nominal estimates  $\bar{\mu}$ ,  $\bar{\psi}_0$ , and  $\bar{\psi}_1$ , and considering

$$\begin{aligned}\mu(x_1, x_2, x_3) &= \bar{\mu}(x_1, x_2, x_3) \left( 1 + a \sum_{i=1}^{L+1} \sum_{j=1}^{L+1} \sum_{k=1}^{L+1} \theta_{i,j,k}^{\mu} \phi_i(x_1) \phi_j(x_2) \phi_k(x_3) \right) \\ \psi_0(x_2, x_3) &= \bar{\psi}_0(x_2, x_3) \left( 1 + a \sum_{j=1}^{L+1} \sum_{k=1}^{L+1} \theta_{j,k}^{\psi_0} \phi_j(x_2) \phi_k(x_3) \right) \\ \psi_1(x_2, x_3) &= \bar{\psi}_1(x_2, x_3) \left( 1 + a \sum_{j=1}^{L+1} \sum_{k=1}^{L+1} \theta_{j,k}^{\psi_1} \phi_j(x_2) \phi_k(x_3) \right)\end{aligned}$$

where  $a = 0.1$  represents the level of uncertainty,  $L = 19$  is an integer specifying a spatial discretization, and  $\phi$  is a linear finite element basis function defined on the interval  $[0, 1]$  with  $L + 1$  equally spaced nodes. Concatenating  $\theta^{\mu}$ ,  $\theta^{\psi_0}$ , and  $\theta^{\psi_1}$  yields a parameter vector  $\theta \in \mathbb{R}^{8800}$ . The discretization of  $Dz^*$  (2), with nominal parameter estimates, i.e.  $\theta = 0$ , is a  $240 \times 8800$  matrix for which we seek its largest singular values and vectors to estimate sensitivity indices.

### 5.3.1 | Accuracy of the randomized GSVD algorithms

The randomized GSVD of (2) is computed with an oversampling factor of  $p = 12$  and  $q = 1$  subspace iteration. The matrix  $S$  arising from the mass matrices defined by inner products of the  $f_i$ 's and the matrix  $T$  arises from the mass matrices defined by inner products of the  $\phi_i$ 's. The generalized singular values of (2) are given in Fig. 8. A low rank structure is identified, where sensitivities in the 8800 dimensional discretized parameter space can be well approximated with small number of singular modes.

### 5.3.2 | Estimating sensitivity indices

Fig. 9 displays the log of the nominal permeability field  $\bar{\mu}$  (left) and the permeability field sensitivity indices (right). In the sensitivity indices panel (right), the size of the dot is scaled by the magnitude of the sensitivity index to aid in visualization of the high sensitivity regions. In particular, we notice a small region of red dots indicating that the high sensitivity is localized to a small region in space.

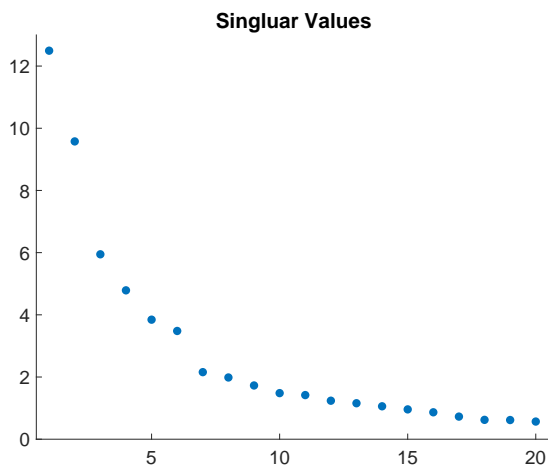


FIGURE 8 The 20 leading generalized singular values of  $Dz^*$ .

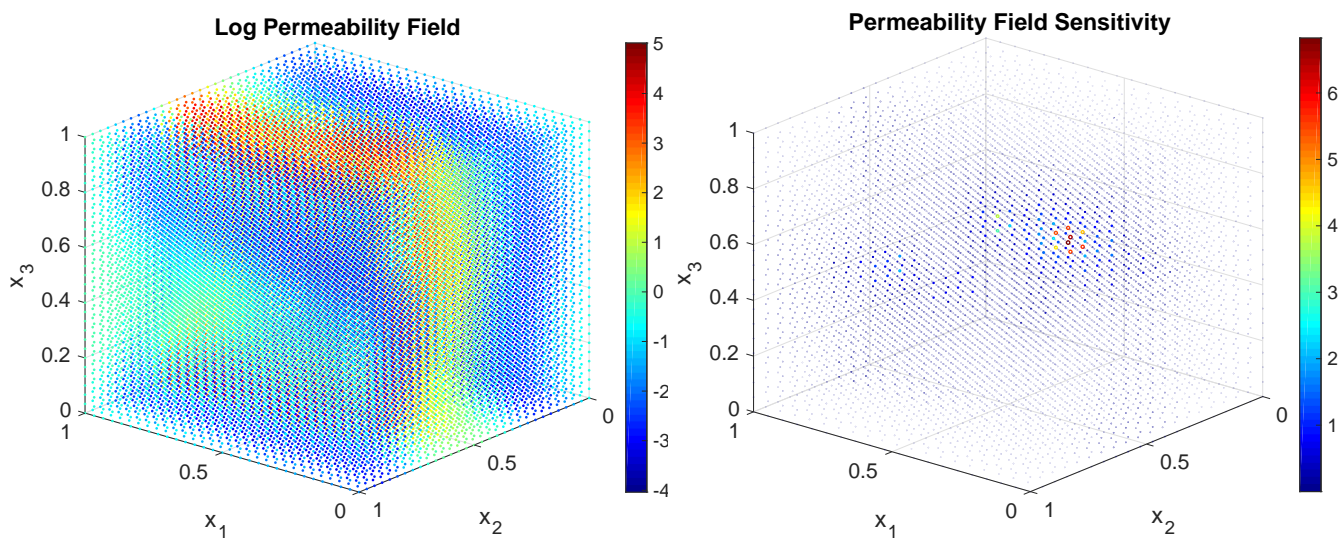
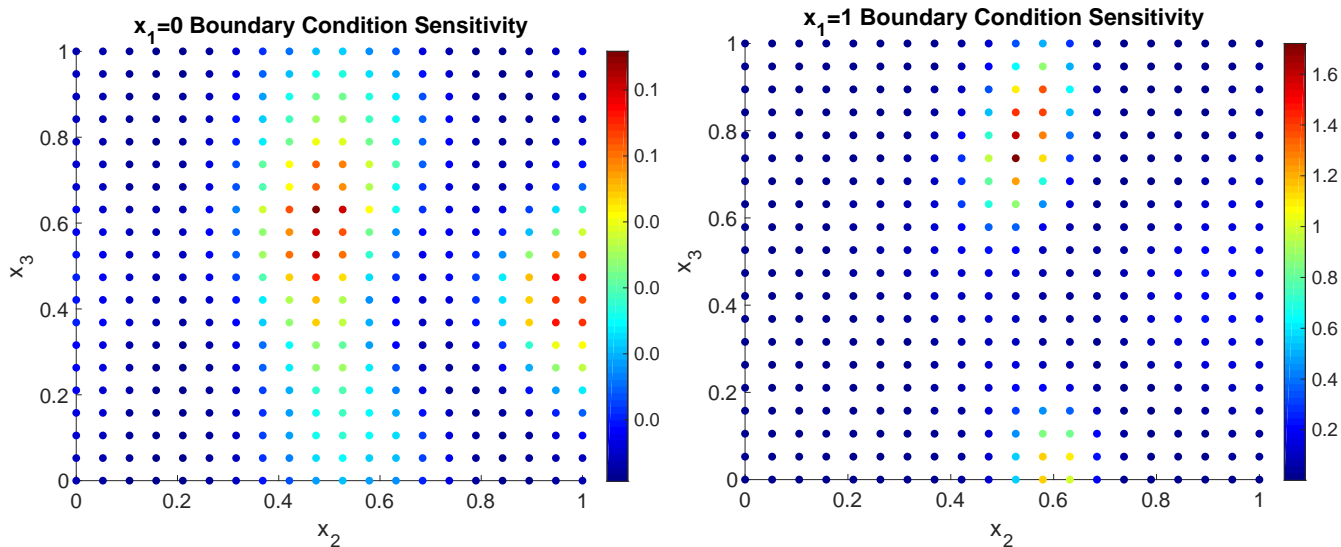


FIGURE 9 Left: natural log of the nominal permeability field  $\bar{\mu}$ ; right: permeability field sensitivity indices.

Fig. 10 displays the boundary condition sensitivity indices corresponding to the  $x_1 = 0$  Dirichlet boundary on the left and  $x_1 = 1$  Dirichlet boundary on the right. We observe spatially localized sensitivity in the boundary conditions. The sensitivity on the  $x_1 = 1$  boundary is an order of magnitude larger than on the  $x_1 = 0$  boundary, while both boundary sensitivities are smaller than the largest permeability field sensitivity indices.

## 6 | CONCLUSIONS AND FUTURE DIRECTIONS

There are three major contributions in this paper. First, we present a new algorithm for computing the truncated GSVD using randomized subspace iterations and discuss numerical and computational issues associated with its implementation. Second, we present probabilistic analysis of the error in the low-rank representation when a standard Gaussian random matrix is used as the initial guess. This analysis provides insight into the parameters of the algorithm—the number of subspace iterations, and the oversampling parameter. Third, we present an application of our algorithm to computing the sensitivity indices in the HDSA framework, and demonstrate through numerical experiments that our approach is both accurate and computationally efficient. Based on these experiments we recommend using Algorithm 3 with  $q = 1$  subspace iterations. If a preconditioner is available, and solves involving  $T$  are expensive, the error can be further lowered using the approach in Section 4.3.



**FIGURE 10** Left:  $x_1 = 0$  Dirichlet boundary condition sensitivity indices; right:  $x_1 = 1$  Dirichlet boundary condition sensitivity indices.

Computing the truncated GSVD with randomized algorithms facilitates efficient analysis of large linear operators arising in a variety of contexts. This article presented hyper-differential sensitivity analysis where the use of a truncated GSVD has potential to yield a significant reduction in the number of matvecs. Further, the randomized algorithms enables efficient distributed memory parallelism which facilitates computation for large-scale applications.

There are several possible avenues for future exploration. First, the analysis in Section 4 centered on the error in the low-rank approximation. Following the work in [16], one can analyze the accuracy in the singular values and the singular vectors. Second, the algorithms proposed in this paper use standard Gaussian random matrices for the initial guess  $\mathbf{\Omega}$ . Several other choices were proposed in this paper but we did not explore them numerically or analytically. It would be interesting to investigate if the dependence of the error condition number  $\kappa_2(\mathbf{T})$  can be further weakened, either by using and developing new preconditioners, or using a different strategy.

In hyper-differential sensitivity analysis, the matrix  $\mathbf{A}$  was defined implicitly and matvecs involving  $\mathbf{A}$  and its transpose require solving linear systems. If an iterative solver is used, and the iterations are stopped early, then this causes an error in the matvecs. An analysis of the error in the GSVD and developing appropriate stopping criteria would also be interesting to investigate. Similarly, analyzing inexactness from the inconsistency in  $\mathbf{B}$  and its transpose is also worth investigating. In addition, future research may explore parallel load balancing associated with computing matvecs in parallel, and the potential to use information from solves in the first stage of the algorithm to precondition solves in the second stage.

## ACKNOWLEDGMENTS

The work of A.K.S. was supported, in part, by the National Science Foundation through the awards DMS-1821149 and DMS-1745654. This paper describes objective technical results and analysis. Any subjective views or opinions that might be expressed in the paper do not necessarily represent the views of the U.S. Department of Energy or the United States Government. Sandia National Laboratories is a multimission laboratory managed and operated by National Technology and Engineering Solutions of Sandia LLC, a wholly owned subsidiary of Honeywell International, Inc., for the U.S. Department of Energy's National Nuclear Security Administration under contract DE-NA-0003525. SAND2020-1576 J.

## References

- [1] O. Alter, P. O. Brown, and D. Botstein. Generalized singular value decomposition for comparative analysis of genome-scale expression data sets of two different organisms. Proceedings of the National Academy of Sciences, 100(6):3351–3356, 2003.
- [2] Å. Björck. Numerical methods in matrix computations, volume 59. Springer, 2015.
- [3] T. A. Davis and Y. Hu. The University of Florida sparse matrix collection. ACM Transactions on Mathematical Software (TOMS), 38(1):1, 2011.
- [4] Z. Drmac and A. K. Saibaba. The discrete empirical interpolation method: Canonical structure and formulation in weighted inner product spaces. SIAM Journal on Matrix Analysis and Applications, 39(3):1152–1180, 2018.
- [5] G. H. Golub and Q. Ye. Inexact inverse iteration for generalized eigenvalue problems. BIT Numerical Mathematics, 40(4):671–684, 2000.
- [6] M. Gu. Subspace iteration randomization and singular value problems. SIAM Journal on Scientific Computing, 37(3):A1139–A1173, 2015.
- [7] N. Halko, P.-G. Martinsson, and J. A. Tropp. Finding structure with randomness: Probabilistic algorithms for constructing approximate matrix decompositions. SIAM review, 53(2):217–288, 2011.
- [8] P. C. Hansen. Rank-deficient and discrete ill-posed problems: numerical aspects of linear inversion, volume 4. Society for Industrial and Applied Mathematics, 2005.
- [9] J. Hart, B. v. B. Waanders, and R. Herzog. Hyper-differential sensitivity analysis of uncertain parameters in PDE-constrained optimization. Accepted in the International Journal for Uncertainty Quantification. arXiv:1909.07336, 2020.
- [10] R. A. Horn and C. R. Johnson. Matrix analysis. Cambridge university press, 2012.
- [11] A. V. Knyazev and M. E. Argentati. Principal angles between subspaces in an A-based scalar product: algorithms and perturbation estimates. SIAM Journal on Scientific Computing, 23(6):2008–2040, 2002.
- [12] R. M. Larsen. Lanczos bidiagonalization with partial reorthogonalization. DAIMI Report Series, (537), 1998.
- [13] B. R. Lowery and J. Langou. Stability analysis of QR factorization in an oblique inner product. arXiv preprint arXiv:1401.5171, 2014.
- [14] S. P. Ponnappalli, M. A. Saunders, C. F. Van Loan, and O. Alter. A higher-order generalized singular value decomposition for comparison of global mRNA expression from multiple organisms. PloS one, 6(12):e28072, 2011.
- [15] Y. Saad. Iterative methods for sparse linear systems, volume 82. Society for Industrial and Applied Mathematics, 2003.
- [16] A. K. Saibaba. Randomized subspace iteration: Analysis of canonical angles and unitarily invariant norms. SIAM Journal on Matrix Analysis and Applications, 40(1):23–48, 2019.
- [17] A. K. Saibaba and P. K. Kitanidis. Fast computation of uncertainty quantification measures in the geostatistical approach to solve inverse problems. Advances in water resources, 82:124–138, 2015.
- [18] A. K. Saibaba, J. Lee, and P. K. Kitanidis. Randomized algorithms for generalized Hermitian eigenvalue problems with application to computing Karhunen–Loève expansion. Numerical Linear Algebra with Applications, 23(2):314–339, 2016.
- [19] V. Simoncini and D. B. Szyld. Theory of inexact Krylov subspace methods and applications to scientific computing. SIAM Journal on Scientific Computing, 25(2):454–477, 2003.
- [20] J. A. Tropp, A. Yurtsever, M. Udell, and V. Cevher. Practical sketching algorithms for low-rank matrix approximation. SIAM Journal on Matrix Analysis and Applications, 38(4):1454–1485, 2017.

- [21] C. F. Van Loan. Generalizing the singular value decomposition. SIAM Journal on Numerical Analysis, 13(1):76–83, 1976.
- [22] S. Vatankehah, R. A. Renaut, and V. E. Ardestani. Total variation regularization of the 3-D gravity inverse problem using a randomized generalized singular value decomposition. Geophysical Journal International, 213(1):695–705, 2018.
- [23] R. Vershynin. Introduction to the non-asymptotic analysis of random matrices, pages 210–268. Cambridge University Press, 2012.
- [24] H. Xiang and J. Zou. Randomized algorithms for large-scale inverse problems with general Tikhonov regularizations. Inverse Problems, 31(8):085008, 2015.
- [25] Q. Ye and P. Zhang. Inexact inverse subspace iteration for generalized eigenvalue problems. Linear Algebra and its Applications, 434(7):1697–1715, 2011.
- [26] P. Zhu and A. V. Knyazev. Angles between subspaces and their tangents. Journal of Numerical Mathematics, 21(4):325–340, 2013.

